Vibronic theory of a structural phase transition and a tricritical point in IV-VI compounds

Kazuo Sakai
Department of Physics, Faculty of Science, Science University of Tokyo, 1-3 Kagurazaka, Shinjuku, Tokyo, 162, Japan
(Received 6 January 1986)

The vibronic theory of a structural phase transition in IV-VI compounds is reformulated in terms of the mean-field approximation, taking account of the spin-orbit coupling between conduction and valence bands and anharmonic couplings between TA and TO modes. The effect of the electron-hole pair polarization is incorporated into the self-energies of the TA phonon as well as the TO phonon, so as to give the carrier concentration dependence of shear modulus C_{44}. This yields the proper dependence of the ratio ζ of temperature derivatives of the squared TO-phonon frequencies in the cubic and rhombohedral phases on the carrier concentration, and also that of the jump of C_{44} in the acoustic anomaly at the transition point. It is shown that the ratio ζ becomes divergent at the tricritical point, and the TA mode softens at the superheating point (in case of first-order transition) or at the tricritical point. The spin-orbit coupling leads to peculiar structures of Fermi surfaces and to an increase in the electron chemical potential with growth of sublattice displacement. It is also shown in the fourth-order anharmonicity of the TO mode that the lattice anharmonicity is suppressed by the vibronic anharmonicity due to the spin-orbit coupling.

I. INTRODUCTION

During the last quarter of the century, many experimental and theoretical studies were performed to elucidate the basic properties of the IV-VI compound narrow-band-gap semiconductors.[1-6] The semiconducting compounds GeTe, SnTe, PbTe, and their ternary alloys exhibit a ferroelectric transition as they pass from cubic to rhombohedral structures, although their ferroelectric moment is screened out by free carriers. Since the crystal structures in both phases are simple and the electronic band structure is well studied, a microscopic model of the phase transition has been developed, and its predictions have been compared with experiments in some detail.[3,7-11].

In the low-temperature phase of IV-VI compounds, there is a relative displacement $\langle \mathbf{u} \rangle$ of the sublattice along the crystalographic [111] directions. In addition, there is a rhombohedral distortion of elementary cube as illustrated in Fig. 1. The rhombohedral angle α is reduced from 90° due to the shear strains $\langle \epsilon_{xy} \rangle$, $\langle \epsilon_{yz} \rangle$, and $\langle \epsilon_{zx} \rangle$. Thus, we have two kinds of order parameters, $\langle \mathbf{u} \rangle$ and $\langle \epsilon_{ij} \rangle$, in this phase. From the microscopic point of view, these two order parameters result from phonon condensation effects: The order parameters $\langle \mathbf{u} \rangle$ and $\langle \epsilon_{ij} \rangle$ correspond to the nonvanishing thermal averages of phonon coordinates of transverse optic (TO) and acoustic (TA) modes in the long-wavelength limit, respectively.

In IV-VI compounds, the TA and TO modes are linked with each other via electrostrictive coupling, which is quadratic (linear) in TO (TA) mode coordinates. This mode coupling gives rise to the following peculiar phenomena. The first is an acoustic anomaly where the TA sound velocity drops prominently as T_c is approached from above even in the second-order phase transition.[12,13] The second is the occurrence of a tricritical point,[14] observed in $Ge_{1-x}Sn_xTe$: Here a crossover of the first- and second-order transition takes place.[15] The Green-function approach to the coupled phonon system between acoustic and optic modes have been made by Pytte[13] and Katayama and Mills[7,8] in the mean-field theory. Pytte obtained the acoustic anomaly and tricritical-point behavior of order parameters, taking account of a linear momentum dependence in the electrostrictive coupling. On the other hand, Katayama and Mills obtained neither the acoustic anomaly nor the tricritical-point behavior because they assumed a constant electrostrictive coupling. This means that the linear momentum dependence of the electrostrictive coupling plays an essential role for the phase transition in the coupled phonon system between TA and TO modes.

The vibronic model was first established by Kristoffel

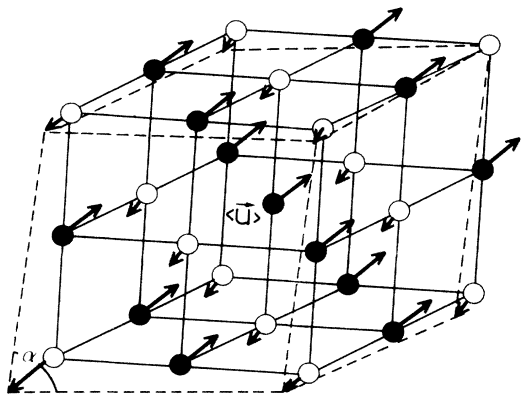

FIG. 1. Crystal structures of IV-VI compounds. The solid and dashed lines denote the structures in high-temperature cubic and low-temperature rhombohedral phases, respectively. The arrow denotes the relative sublattice displacement $\langle \mathbf{u} \rangle$. The rhombohedral angle is denoted by α.

and Konsin[16] and Bersuker and Vekhter[17] to explain the occurrence of ferroelectricity in crystals, and Kawamura *et al.*[18] were the first to apply it to the IV-VI semiconducting compounds. It is noted that the driving mechanism for ferroelectricity is still controversial,[19–21] whether the vibronic mechanism is responsible for it or not. The different microscopic models have also been discussed,[22] one of which is the polarizability model[11] based on the local nonlinear electron-ion interaction of the chalcogenide ions. Here we adopt the vibronic mechanism as the cause of the ferroelectric instability. This leads to understanding the structural phase transition in IV-VI compounds from the semiconductor approach.

In the ferroelectric phase transition, the TO phonon softens at the Γ point where the TO mode has a definite odd parity. This mode combines the conduction and valence states of different parities and gives rise to the unstable cubic phase. In the terminology of the many-body theory, this is caused by the particle-hole pair excitation due to the electron–TO-phonon interaction.[2] In IV-VI compounds, the electronic states with definite parity are located at the L points with a direct gap of a few tenths of an eV.[23] The conduction and valence bands near these L points are well described in terms of the $\mathbf{k}\cdot\mathbf{p}$ perturbational two-band model because the narrow band gaps are so distinctive.[24,25] It is important to note here that these bands are strongly nonparabolic due to large spin-orbit coupling. In fact, the spin-orbit coupling energy (of the order of 1 eV or less[24]) is larger than the band gap, and induces the interband mixing through the velocity matrix elements. The electron TO- (TA-) phonon coupling constant has only interband (intraband) matrix elements, and the TO mode competes with spin-orbit coupling while the TA mode does not. Inclusion of spin-orbit coupling then leads to splitting of Kramers doublet due to a breakdown of an inversion symmetry, caused by the relative sublattice displacement $\langle\mathbf{u}\rangle$. This induces a distortion of Fermi surfaces in the rhombohedral phase.[9,26].

Prominent carrier concentration dependence is observed in the transition temperature[27,28] and the shear modulus C_{44} of SnTe.[29] This is thus far attributed to the electron-hole polarization of TO-phonon mode which is responsible for the instability of the cubic phase.[2,3,8,30,31] In the present paper, we incorporate the concentration dependence of the shear modulus C_{44} into vibronic theory as the effects of particle-hole pair polarization in the TA mode. It will be seen that this affects the nature of the phase transition as well as the strength of the electrostrictive coupling. Specifically, the following quantities characterizing the transition become dependent on the carrier concentration: the ratio of the temperature derivatives of the squared TO-phonon frequencies in the cubic and rhombohedral phases and the jump of the shear modulus in the acoustic anomaly at the transition point. Some of the results of the present paper have been reported elsewhere.[32]

The plan of the paper is as follows. In Sec. II we describe our model and assumptions in some detail. In Sec. III, the modification of phonon states due to static distortions in the rhombohedral phase is described, and the self-consistent equations of these static distortions are derived and analyzed in Sec. IV. Based on these equations, the behavior of the soft TO mode, the acoustic anomaly, and the modification of electronic states are discussed in Secs. V, VI, and VII, respectively. In Sec. VIII, our theory is compared with experiments of SnTe and $Pb_{1-x}Ge_xTe$. A physical interpretation of the results of the paper are summarized in Sec. IX.

II. MODEL AND ASSUMPTIONS

A. Two-band electron with spin-orbit coupling

As stressed in the Introduction, the spin-orbit interaction plays an important role in determining the band structures of narrow-band-gap semiconductors. The free motion of an electron in such a system is described by the Hamiltonian

$$H_{\rm el}=\int d\mathbf{r}\hat{\psi}^{\dagger}(\mathbf{r})\hat{h}_{\rm el}\hat{\psi}(\mathbf{r})$$
$$=\int d\mathbf{r}\hat{\psi}^{\dagger}(\mathbf{r})\left[\frac{\mathbf{p}^2}{2m}+V_p+\frac{1}{8m^2c^2}\nabla^2V_p+\frac{1}{4m^2c^2}\boldsymbol{\sigma}\times\nabla V_p\cdot\mathbf{p}\right]\hat{\psi}(\mathbf{r}), \quad (2.1)$$

where $V_p(\mathbf{r})$ is the periodic crystal potential, $\boldsymbol{\sigma}$ is the Pauli spin matrices representing electron spin, and $\hat{\psi}(\mathbf{r})$ is the electron field operator.

In the cubic phase, the electron bands derived from Eq. (2.1) have their extrema at the L points $\mathbf{k}=\mathbf{k}^j$ $(j=1,\ldots,4)$ on the four equivalent [111] axes of the Brillouin zone. At each of these L points, the eigenstates of the conduction and valence bands are given by a set of four band-edge wave functions $\phi_{c\mathbf{k}^j\sigma}$ and $\phi_{v\mathbf{k}^j\sigma}$ with doubly degenerate eigenvalues E_c and E_v (Kramers doublets). Here the subscript σ denote different states α and β in the Kramers doublets on the conduction (c) and valence (v) bands. Hereafter the electronic energy is measured from the center of the band gap $(E_c+E_v)/2$. We work in the units $\hbar=k_B=1$, and the crystal volume V is assumed to be unity.

It is shown by band-structure calculations in SnTe (Refs. 33–36) and GeTe (Ref. 37) that the minimum band gap is not at the L point but that at L one finds a saddle point. This effect on the structural phase transition is discussed by Dugaev *et al.*[38] within the framework of an isotropic Kane model neglecting spin-orbit coupling. Their isotropic Kane model study overestimates its effect compared to the model including the spin-orbit coupling because of the overestimation of the phase volume at the extremum. The prominent effect would be seen when the spin-orbit coupling is explicitly taken into account, such as in the diamagnetic susceptibility[39,40] which is not discussed here. We hereafter assume the minimum gap is located at L point for simplicity.

Let us introduce the modified Luttinger-Kohn functions,[25,41]

$$\chi^j_{l\mathbf{k}\sigma}(\mathbf{r})=e^{i(\mathbf{k}-\mathbf{k}^j)\cdot\mathbf{r}}\phi_{l\mathbf{k}^j\sigma}(\mathbf{r}), \quad (2.2)$$

to represent the states $\mathbf{k}$ in the vicinity of the L points $\mathbf{k}^j$, and make use of these functions to expand the electron field operator $\hat{\psi}(\mathbf{r})$ in the form

$$\hat{\psi}(\mathbf{r})=\sum_j \sum_{l,\mathbf{k},\sigma} \chi^j_{l\mathbf{k}\sigma}(\mathbf{r})\hat{a}^j_{l\mathbf{k}\sigma} . \tag{2.3}$$

The operator $\hat{a}^j_{l\mathbf{k}\sigma}$ [$(\hat{a}^j_{l\mathbf{k}\sigma})^\dagger$] annihilates (creates) an electron in the state $(l,\mathbf{k},\sigma)$ near the jth L point. Throughout the paper, we neglect the effects of intervalley transitions. Except for $\mathbf{k}=\mathbf{k}^j$, the wave functions (2.2) are not the eigenfunctions of the single-electron Hamiltonian $\hat{h}_{\rm el}$ in Eq. (2.1). The second quantized version of the Hamiltonian in the $\mathbf{k}\cdot\mathbf{p}$ perturbational two-band model is thus expressed in the form[25]

$$H_{\rm el}=\sum_j \sum_{\mathbf{k}} [(\hat{a}^j(\mathbf{k})]^\dagger \hat{E}^j(\mathbf{k})\hat{a}^j(\mathbf{k}) , \tag{2.4}$$

where a 4×4 matrix $\hat{E}^j(\mathbf{k})$ is introduced by

$$\hat{E}^j(\mathbf{k})=\Delta\hat{\gamma}_0+i\boldsymbol{\kappa}^j\cdot\hat{\boldsymbol{\gamma}} , \tag{2.5}$$

to express the matrix elements of $\hat{h}_{\rm el}$ with respect to the wave functions (2.2). Here Δ stands for the half band gap $E_G/2=(E_c-E_v)/2$, and $\hat{\gamma}_n$ $(n=0,\ldots,3)$ are Dirac's γ matrices[42]

$$\hat{\gamma}_0=\begin{bmatrix} \underline{1} & \underline{0} \\ \underline{0} & -\underline{1} \end{bmatrix}, \quad \hat{\gamma}_n=\begin{bmatrix} \underline{0} & \sigma_n \\ -\sigma_n & \underline{0} \end{bmatrix} , \tag{2.6}$$

where $\underline{1}$ is 2×2 unit matrix and σ_n denote the Pauli spin matrices. Note that the indices of these matrices indicate the labels c, v and the labels of Kramers states α, β. Details for the γ matrix are referred to in Ref. 42.

The nth component of modified crystal momentum $\kappa^j(n)$ is defined by

$$\kappa^j_n=(\mathbf{k}-\mathbf{k}^j)\cdot\mathbf{W}^j(n) , \tag{2.7}$$

where the vectors $\mathbf{W}^j(n)$ represent the matrix elements of the velocity operator $\boldsymbol{\pi}/m=\mathbf{p}/m+[1/(4m^2c^2)]\boldsymbol{\sigma}\times\nabla V_p$ in the presence of spin-orbit interaction:[25]

$$\mathbf{W}^j(1)=\mathrm{Im}\langle\phi_{c\mathbf{k}^j\alpha}|\boldsymbol{\pi}|\phi_{v\mathbf{k}^j\beta}\rangle/m , \tag{2.8a}$$

$$\mathbf{W}^j(2)=\mathrm{Re}\langle\phi_{c\mathbf{k}^j\alpha}|\boldsymbol{\pi}|\phi_{v\mathbf{k}^j\beta}\rangle/m , \tag{2.8b}$$

$$\mathbf{W}^j(3)=\mathrm{Im}\langle\phi_{c\mathbf{k}^j\alpha}|\boldsymbol{\pi}|\phi_{v\mathbf{k}^j\alpha}\rangle/m . \tag{2.8c}$$

B. Interacting TA and TO phonons

The relative sublattice displacement $u(\mathbf{r})$ and rhombohedral shear strain $\epsilon_{ij}(\mathbf{r})$ are related to the transverse optic (TO) and transverse acoustic (TA) phonons, respectively. Let us express these in terms of phonon coordinates $Q_{\mathbf{q}}$ and $Q^a_{\mathbf{q}}$:

$$\mathbf{u}(\mathbf{r})=\frac{1}{\sqrt{NM}}\sum_{\mathbf{q}}\mathbf{e}(\mathbf{q})Q_{\mathbf{q}}e^{i\mathbf{q}\cdot\mathbf{r}} , \tag{2.9}$$

$$\epsilon_{ij}(\mathbf{r})=\frac{1}{\sqrt{\rho}}\sum_{\mathbf{q}}|\tilde{\epsilon}_{ij}(0)|qQ^a_{\mathbf{q}}e^{i\mathbf{q}\cdot\mathbf{r}} . \tag{2.10}$$

In Eq. (2.9), $\mathbf{e}(\mathbf{q})$ denotes the polarization vector of TO phonon with wave vector $\mathbf{q}$, N the number of the unit cells, and M the reduced mass in the unit cell. We have replaced in Eq. (2.10) the TA-phonon coordinates $Q^a_{\mathbf{q}}$ by $[\tilde{\epsilon}_{ij}(\mathbf{q})/|\tilde{\epsilon}_{ij}(0)|]Q^a_{\mathbf{q}}$ for simplicity, and $\tilde{\epsilon}_{ij}(\mathbf{q})$ is defined by

$$\tilde{\epsilon}_{ij}(q)=\frac{i}{2q}[q_ie_j(\mathbf{q})+q_je_i(\mathbf{q})] , \tag{2.11}$$

where $e_i(\mathbf{q})$ is the polarization vector of the TA phonon with wave vector $\mathbf{q}$, and ρ is the mass density of the crystal. The above definition is meaningful when $qQ^a_{\mathbf{q}}$ has a finite value in the limit $q\to0$. This requires an implicit q dependence of the type $Q^a_{\mathbf{q}}\propto1/q$ in the long-wavelength limit. Such a q dependence is naturally expected, if we consider the thermal average of the operator $(Q^a_{\mathbf{q}})^\dagger Q^a_{\mathbf{q}}$ in the long-wavelength limit:

$$\langle(Q^a_{\mathbf{q}})^\dagger Q^a_{\mathbf{q}}\rangle=\frac{1}{qs_0}\coth\frac{qs_0}{2T}\to\frac{1}{q^2}\frac{2T}{s_0^2} \quad \text{as } \mathbf{q}\to\mathbf{0} , \tag{2.12}$$

where s_0 is the sound velocity of TA mode at the Γ point. This relation clearly shows that $qQ^a_{\mathbf{q}}$ is nonvanishing in the limit $q\to0$, and the static homogeneous strain $\langle\epsilon_{ij}\rangle\neq0$ is possible in the presence of the thermal average $\langle Q^a_{\mathbf{q}}\rangle\neq0$.

In the absence of the interactions between the different modes and with electrons, the motions of TA and TO phonons are described by

$$H_{\rm TA}=\tfrac{1}{2}\sum_{\mathbf{q}}(P^a_{\mathbf{q}})^\dagger P^a_{\mathbf{q}}+\tfrac{1}{2}\sum_{\mathbf{q}}q^2s_0^2(Q^a_{\mathbf{q}})^\dagger Q^a_{\mathbf{q}} , \tag{2.13}$$

$$H_{\rm TO}=\tfrac{1}{2}\sum_{\mathbf{q}}P^\dagger_{\mathbf{q}}P_{\mathbf{q}}+\tfrac{1}{2}\sum_{\mathbf{q}}\omega_q^2Q^\dagger_{\mathbf{q}}Q_{\mathbf{q}}+\frac{1}{4!}\sum_{\mathbf{q}_1,\ldots,\mathbf{q}_4}A(\mathbf{q}_1,\mathbf{q}_2,\mathbf{q}_3,\mathbf{q}_4)\Delta(\mathbf{q}_1+\cdots+\mathbf{q}_4)Q_{\mathbf{q}_1}Q_{\mathbf{q}_2}Q_{\mathbf{q}_3}Q_{\mathbf{q}_4} . \tag{2.14}$$

Here $\omega_{\mathbf{q}}$ and qs_0 are the frequencies of TO and TA phonons in the harmonic approximation, the second terms in Eq. (2.14) represent the interaction among the TO phonons, and $\Delta(\cdots)$ symbolizes conservation of crystal momenta.[43]

In order to guarantee the coexistence of order parameters $\langle\mathbf{u}\rangle$ and $\langle\epsilon_{ij}\rangle$, we have to introduce the coupling between TA- and TO-phonon modes. Symmetry consideration leads us to the following form for this interaction:[12]

$$H_{\text{TA-TO}}=\tfrac{1}{2}\sum_{\mathbf{q}_1,\mathbf{q}_2,\mathbf{q}_3}B(\mathbf{q}_1,\mathbf{q}_2,\mathbf{q}_3)\Delta(\mathbf{q}_1+\mathbf{q}_2+\mathbf{q}_3)q_1Q^a_{\mathbf{q}_1}Q_{\mathbf{q}_2}Q_{\mathbf{q}_3}$$
$$+\tfrac{1}{4}\sum_{\mathbf{q}_1,\ldots,\mathbf{q}_4}C(\mathbf{q}_1,\mathbf{q}_2,\mathbf{q}_3,\mathbf{q}_4)\Delta(\mathbf{q}_1+\cdots+\mathbf{q}_4)q_1q_2Q^a_{\mathbf{q}_1}Q^a_{\mathbf{q}_2}Q_{\mathbf{q}_3}Q_{\mathbf{q}_4} . \tag{2.15}$$

Here the first term represents the electostrictive coupling responsible for the acoustic anomaly[12,13] as well as the appearance of the tricritical point, while the second term is introduced to give the proper temperature dependence of TO-phonon frequency.[3] In the above, we have assumed that there are only a single branch of TA or TO modes. This simplification does not alter the essence of our results, although there are several branches for these phonon modes in the real systems.

C. Electron-phonon interactions

We have to take into account the effects of electron-phonon interaction in order to understand the observed dependence of transition temperature on the free carrier concentration. To derive the coupling between electron and TO phonons, we expand the periodic crystal potential $V_p(\mathbf{r})$ in powers of the displacement $\mathbf{u}(\mathbf{r})$.[44] Retaining the lowest-order terms, the matrix elements are calculated, and we obtain

$$H_{\text{el-TO}}=\sum_{j,\mathbf{k},\mathbf{q}}(2\omega_{\mathbf{q}})^{1/2}[\hat{a}^{j}(\mathbf{k}+\mathbf{q})]^{\dagger}\hat{g}^{j}(\mathbf{q})\hat{a}^{j}(\mathbf{k})Q_{\mathbf{q}} . \quad (2.16)$$

Here the elements of the 4×4 matrix,

$$\hat{g}^{j}(\mathbf{q})=\mathbf{g}^{j}\cdot\hat{\gamma}_0\hat{\gamma} , \quad (2.17)$$

represent various channels of interband transition of electrons, absorbing or emitting a single TO phonon. The components of the vector g_n^j are related to the optic deformation potentials $\Xi^j(n)$'s ($n=1,2$ and 3) by

$$g_n^j=-\frac{1}{(2NM\omega_q)^{1/2}}\mathbf{e}(\mathbf{q})\cdot\Xi^j(n) , \quad (2.18)$$

where contribution from the Umklapp processes have been neglected.[41] The expressions and properties of $\Xi^j(n)$ are summarized in Appendix A.

Finally, we assume the presence of an additional energy proportional to the local rhombohedral strain $\epsilon_{ij}(\mathbf{r})$ and the electron density. This gives the electron—TA-phonon interaction of the form

$$H_{\text{el-TA}}=\sum_{j,\mathbf{k},\mathbf{q}}(2qs_0)^{1/2}[\hat{a}^{j}(\mathbf{k}+\mathbf{q})]^{\dagger}\hat{f}^{j}(\mathbf{q})\hat{a}^{j}(\mathbf{k})Q_{\mathbf{q}}^{a} . \quad (2.19)$$

The elements of $\hat{f}^{j}(\mathbf{q})$ represent the intraband transitions of electron due to absorption or emission of a TA-phonon, and are related to the acoustic deformation potential Ξ_{nm}^{lj} by

$$\hat{f}^{j}(\mathbf{q})_{l\sigma l\sigma}=-\frac{q}{(2qs_0\rho)^{1/2}}\sum_{n,m}\Xi_{nm}^{lj}\tilde{\epsilon}_{nm}(0) \equiv\frac{q}{(2qs_0)^{1/2}}[\hat{\tilde{f}}^{j}(0)]_{l\sigma l\sigma} , \quad (2.20)$$

where the factor $\tilde{\epsilon}_{nm}(\mathbf{q})$ is defined in Eq. (2.11). Further details for these quantities are given in Appendix A.

Summarizing, our system consists of mutually interacting two-band electrons and two modes of phonons, described by the total Hamiltonian

$$H=H_{\text{el}}+H_{\text{el-TA}}+H_{\text{el-TO}}+H_{\text{TA}}+H_{\text{TO}}+H_{\text{TA-TO}} . \quad (2.21)$$

III. STATIC DISTORTIONS IN RHOMBOHEDRAL PHASE

The rhombohedral phase is characterized by the presence of static uniform distortions $\langle\mathbf{u}\rangle$ and $\langle\epsilon_{ij}\rangle$. It is known that the sublattice displacement $\langle\mathbf{u}\rangle$ is induced along the [111] axis:

$$\langle u_x\rangle=\langle u_y\rangle=\langle u_z\rangle\equiv\langle u\rangle,\quad \mathbf{e}(0)=\frac{1}{\sqrt{3}}(1,1,1) . \quad (3.1)$$

On the other hand, the nonvanishing elements of shear strain are given by

$$\langle\epsilon_{xy}\rangle=\langle\epsilon_{yz}\rangle=\langle\epsilon_{zx}\rangle\equiv\langle\epsilon\rangle,\quad |\tilde{\epsilon}_{ij}(0)|=\frac{1}{\sqrt{12}} . \quad (3.2)$$

The static strain $\langle\epsilon\rangle$ is related to the rhombohedral angle α by $\alpha=90^\circ-2\langle\epsilon\rangle$.

Thus we have two order parameters in this phase to be determined self-consistently. It is clear that these order parameters are related to the averages of phonon coordinates $Q_{\mathbf{q}}$ and $qQ_{\mathbf{q}}^{a}$ in the limit $\mathbf{q}=\mathbf{0}$:

$$\langle Q_{\mathbf{q}}\rangle\to\sqrt{3NM}\,\langle u\rangle\equiv\tilde{u} ,$$
$$\langle qQ_{\mathbf{q}}^{a}\rangle\to\sqrt{12\rho}\langle\epsilon\rangle\equiv\tilde{\epsilon},\quad q\to0 . \quad (3.3)$$

Then it will be convenient to introduce the new phonon coordinates

$$Q'_{\mathbf{q}}=Q_{\mathbf{q}}-\tilde{u}\delta_{\mathbf{q},0},\quad q(Q_{\mathbf{q}}^{a})'=qQ_{\mathbf{q}}^{a}-\tilde{\epsilon}\delta_{\mathbf{q},0} , \quad (3.4)$$

to denote the vibrations around displaced centers. When the Hamiltonian (2.21) is expressed in terms of these new coordinates, the follow modifications are needed.

(1) The changes in the elastic energies due to static distortions give a constant term

$$E_0=\tfrac{1}{2}\omega_0^2\tilde{u}^2+\tfrac{1}{2}s_0^2\tilde{\epsilon}^2+\frac{1}{4!}A\tilde{u}^4+\tfrac{1}{2}B\tilde{\epsilon}\tilde{u}^2+\tfrac{1}{4}C\tilde{\epsilon}^2\tilde{u}^2 , \quad (3.5)$$

where A, B, and C are the coupling constants with vanishing momenta.

(2) The self-energy correction of the form

$$\hat{\Sigma}^{j}=(2\omega_0)^{1/2}\tilde{u}\hat{g}^{j}(0)+\tilde{\epsilon}\hat{\tilde{f}}^{j}(0) , \quad (3.6)$$

should be added to electron band energy matrix $\hat{E}^{j}(\mathbf{k})$ in Eq. (2.4). Here $\hat{\tilde{f}}^{j}(0)$ is defined in Eq. (2.20).

(3) The sound velocity s_0 of the TA phonon and TO-phonon frequency in Eqs. (2.13) and (2.14) are to be replaced by

$$(s_0')^2=\frac{\partial^2E_0}{\partial\tilde{\epsilon}^2},\quad (\omega_{\mathbf{q}}')^2=\frac{\partial^2E_0}{\partial\tilde{u}^2} . \quad (3.7)$$

(4) An additional term

$$\delta H_{\text{TO}}=\tilde{u}\frac{1}{3!}\sum_{\mathbf{q}_1,\mathbf{q}_2,\mathbf{q}_3}A(\mathbf{q}_1,\mathbf{q}_2,\mathbf{q}_3,0)\Delta(\mathbf{q}_1+\mathbf{q}_2+\mathbf{q}_3)Q_{\mathbf{q}_1}Q_{\mathbf{q}_2}Q_{\mathbf{q}_3} , \quad (3.8)$$

is to be added to H_{TO} in Eq. (2.14), and

$$\delta H_{\mathrm{TA\text{-}TO}}=\tilde{u}\sum_{\mathbf{q}}[B(\mathbf{q},-\mathbf{q},0)+\tilde{\epsilon}C(0,\mathbf{q},-\mathbf{q},0)]q(Q^a_{\mathbf{q}})^{\dagger}Q_{\mathbf{q}}$$
$$+\tfrac{1}{2}\tilde{u}\sum_{\mathbf{q}_1,\mathbf{q}_2,\mathbf{q}_3}C(\mathbf{q}_1,\mathbf{q}_2,\mathbf{q}_3,0)\Delta(\mathbf{q}_1+\mathbf{q}_2+\mathbf{q}_3)q_1q_2Q^a_{\mathbf{q}_1}Q^a_{\mathbf{q}_2}Q_{\mathbf{q}_3}$$
$$+\tfrac{1}{2}\tilde{\epsilon}\sum_{\mathbf{q}_1,\mathbf{q}_2,\mathbf{q}_3}C(0,\mathbf{q}_1,\mathbf{q}_2,\mathbf{q}_3)\Delta(\mathbf{q}_1+\mathbf{q}_2+\mathbf{q}_3)q_1Q^a_{\mathbf{q}_1}Q_{\mathbf{q}_2}Q_{\mathbf{q}_3}\ , \tag{3.9}$$

to $H_{\mathrm{TA\text{-}TO}}$ in Eq. (2.15). The primes on the new coordinates are omitted hereafter.

It is important to note the appearance of the terms, linearly proportional to the uniform fluctuations of TO and TA phonons:

$$\left[\frac{\partial E_0}{\partial\tilde{u}}+\sum_{j,k}[\hat{a}^j(\mathbf{k})]^{\dagger}(2\omega_0)^{1/2}\hat{g}^j(0)\hat{a}^j(\mathbf{k})\right]Q_0+\left[\frac{\partial E_0}{\partial\tilde{\epsilon}}+\sum_{j,k}[\hat{a}^j(\mathbf{k})]^{\dagger}\hat{\tilde{f}}^j(0)\hat{a}^j(\mathbf{k})\right](qQ^a_{\mathbf{q}})_{\mathbf{q}\to 0}\ . \tag{3.10}$$

Here, each coefficient of the operator Q_0 and $(qQ^a_{\mathbf{q}})_{\mathbf{q}\to 0}$ represents the total static force on the distorted lattice. In addition to these, the lattice suffers the forces from the thermally excited phonons in the finite temperature. Then we can derive the self-consistency conditions for the order parameters $\tilde{u}$ and $\tilde{\epsilon}$ by requiring that the thermal averages of these forces vanish. Making use of the equations of motion for $Q_{\mathbf{q}}$ and $qQ^a_{\mathbf{q}}$, one can derive the self-consistency conditions for $\tilde{u}$ and $\tilde{\epsilon}$ in the form

$$\frac{\partial E_0}{\partial\tilde{u}}+\sum_{j,k}\langle[\hat{a}^j(\mathbf{k})]^{\dagger}(2\omega_0)^{1/2}\hat{g}^j(0)\hat{a}^j(\mathbf{k})\rangle+\tfrac{1}{2}\tilde{u}\sum_{\mathbf{q}}A(\mathbf{q},-\mathbf{q},0,0)\langle Q^{\dagger}_{\mathbf{q}}Q_{\mathbf{q}}\rangle$$
$$+\tfrac{1}{2}\tilde{u}\sum_{\mathbf{q}}C(\mathbf{q},-\mathbf{q},0,0)q^2\langle(Q^a_{\mathbf{q}})^{\dagger}Q^a_{\mathbf{q}}\rangle+\sum_{\mathbf{q}}[B(\mathbf{q},-\mathbf{q},0)+\tilde{\epsilon}C(0,\mathbf{q},-\mathbf{q},0)]q\langle Q^{\dagger}_{\mathbf{q}}Q^a_{\mathbf{q}}\rangle=0\ , \tag{3.11}$$

$$\frac{\partial E_0}{\partial\tilde{\epsilon}}+\sum_{j,k}\langle[\hat{a}^j(\mathbf{k})]^{\dagger}\hat{\tilde{f}}^j(0)\hat{a}^j(\mathbf{k})\rangle+\tilde{u}\sum_{\mathbf{q}}C(0,\mathbf{q},-\mathbf{q},0)q\langle Q^{\dagger}_{\mathbf{q}}Q^a_{\mathbf{q}}\rangle+\tfrac{1}{2}\sum_{\mathbf{q}}[B(0,\mathbf{q},-\mathbf{q})+\tilde{\epsilon}C(0,0,\mathbf{q}-\mathbf{q})]\langle Q^{\dagger}_{\mathbf{q}}Q_{\mathbf{q}}\rangle=0\ . \tag{3.12}$$

IV. TRANSITION TEMPERATURE AND ORDER PARAMETERS

In order to determine the order parameters $\tilde{\epsilon}$ and $\tilde{u}$, we have to calculate various thermal averages in Eqs. (3.11) and (3.12). Thermal Green functions for both electrons and phonons are useful for this aim as well as for the discussion of softening of TO phonons and acoustic anomaly in TA mode.[13] Leaving rather lengthy details of the method in Appendix B, we are going to write down here only the results with comments on the associated assumptions and approximations.

The calculation of thermal averages in the self-consistent conditions (3.11) and (3.12) are performed as follows.

(1) The second terms in these equations represent the self-energy parts of the homogeneous TO and TA modes due to virtual polarization of two-band electron gas. These are expressed in terms of the one-electron Green function $\hat{G}^j(\mathbf{k};i\omega_n)$, for example,

$$\sum_{j,k}\langle[\hat{a}^j(\mathbf{k})]^{\dagger}(2\omega_0)^{1/2}\hat{g}^j(0)\hat{a}^j(\mathbf{k})\rangle$$
$$=T\sum_n e^{i\omega_n 0^+}\sum_{j,\mathbf{k}}\mathrm{Tr}[(2\omega_0)^{1/2}\hat{g}^j(0)\hat{G}^j(\mathbf{k};i\omega_n)]\ . \tag{4.1}$$

In treating the electronic states, we regard the static self-energy correction (3.6) as the most dominant effect, and leave out all other effects such as the self-energy due to virtual excitation of thermal phonons. Thus

$$\hat{G}^j(\mathbf{k};i\omega_n)=[i\omega_n+\mu-\hat{E}^j(\mathbf{k})-\hat{\Sigma}^j]^{-1} \tag{4.2a}$$
$$=\hat{G}^j_0(\mathbf{k};i\omega_n)+\hat{G}^j_0(\mathbf{k};i\omega_n)\hat{\Sigma}^j\hat{G}^j_0(\mathbf{k};i\omega_n)\ , \tag{4.2b}$$

where $\hat{G}^j_0(\mathbf{k};i\omega_n)=[i\omega_n+\mu-\hat{E}^j(\mathbf{k})]^{-1}$ describes an electron in the unperturbed two bands. Substitution of expanded form (4.2b) into (4.1) gives a contribution $-\tilde{u}\Pi_{\mathrm{TO}}$ where Π_{TO} is defined by

$$\Pi_{\mathrm{TO}}=-T\sum_n e^{i\omega_n 0^+}\sum_{j,\mathbf{k}}\mathrm{Tr}[(2\omega_0)^{1/2}\hat{g}^j(0)\hat{G}^j_0(\mathbf{k};i\omega_n)(2\omega_0)^{1/2}\hat{g}^j(0)\hat{G}^j_0(\mathbf{k};i\omega_n)]$$
$$=\frac{2\kappa_0}{3\pi^2NMv_{\parallel}v_{\perp}^2}\Xi_{\mathrm{op}}^2\left[1+3\frac{\Delta^2}{\kappa_0^2}\ln\frac{2\kappa_0}{|\mu|+(\mu^2-\Delta^2)^{1/2}}-\frac{1}{\kappa_0^2}|\mu|(\mu^2-\Delta^2)^{1/2}-4\frac{\Delta^2}{\kappa_0^2}\left[1-\frac{(\mu^2-\Delta^2)^{1/2}}{|\mu|}\right]\right]\ , \tag{4.3}$$

and is expressed by the first diagram in Fig. 6(e). Similarly the second term in Eq. (3.12) is shown to yield the contribution $-\tilde{\epsilon}\Pi_{\mathrm{TA}}$, and Π_{TA} is expressed in the form

$$\Pi_{\rm TA}=-\sum_{j,\mathbf{k}} T\sum_n {\rm Tr}[\hat{\tilde{f}}^j(0)\hat{G}^j_0(\mathbf{k};i\omega_n)\hat{\tilde{f}}^j(0)\hat{G}^j_0(\mathbf{k};i\omega_n)]e^{i\omega_n 0^+}$$
$$=-\frac{1}{18\pi^2\rho v_{\parallel}v_{\perp}^2}\left[[2(\Xi_+^{(1)})^2+(\Xi_-^{(1)})^2]\,|\mu|\,(\mu^2-\Delta^2)^{1/2}-(\Xi_-^{(1)})^2\Delta^2\ln\frac{|\mu|+(\mu^2-\Delta^2)^{1/2}}{|\Delta|}\right]. \tag{4.4}$$

In deriving Eqs. (4.3) and (4.4), we have made use of the identity

$${\rm Tr}[\hat{g}^j(0)\hat{G}^j_0(\mathbf{k};i\omega_n)\hat{\tilde{f}}^j(0)\hat{G}^j_0(\mathbf{k};i\omega_n)]=0\,. \tag{4.5}$$

(2) A simple Bose distribution with bare frequency ω_q is assumed to calculate the average $\langle Q_{\rm q}^\dagger Q_{\rm q}\rangle$.[13,45] Inclusion of the correction $\partial^2 E_0/\partial\tilde{u}^2$ is shown to lead to a minor renormalization of various anharmonic phonon coupling constants. In evaluating the average $\langle(Q_{\rm q}^a)^\dagger Q_{\rm q}^a\rangle$, we have taken account of the frequency shift of TA phonons, coming from the polarization of two-band electrons. This gives the carrier concentration dependence of the shear elastic constant C_{44},[29] as will be discussed in Sec. VI.

(3) The cross mode average $\langle Q_{\rm q}^\dagger Q_{\rm q}^a\rangle$ represents the effect of electrostrictive coupling B. As is shown in Appendix B, this yields a term proportional to a strongly temperature-dependent function $F_{\rm TA}(T)$ which appears in the expression of $\langle(Q_{\rm q}^a)^\dagger Q_{\rm q}^a\rangle$.

(4) The anharmonic coupling constants are assumed to have the following momentum dependence:

$$A(\mathbf{q},-\mathbf{q},0,0)=A\phi(\mathbf{q})\,, \tag{4.6a}$$
$$B(\mathbf{q},-\mathbf{q},0)=B\sqrt{\phi(\mathbf{q})}\,, \tag{4.6b}$$
$$C(\mathbf{q},-\mathbf{q},0,0)=C\phi(\mathbf{q})\,, \tag{4.6c}$$

where

$$\phi(\mathbf{q})=\frac{1}{1+(q\eta/q_D)^2}\,, \tag{4.7}$$

q_D is the Debye momentum $2\pi/a$, and η is the smallness parameter to fit the expermental data. The meaning of this choice of momentum dependence of the anharmonic coupling constants will be discussed in Sec. IX.

Summarizing these results, the self-consistency condition (3.11) can be written as

$$\frac{\partial E_0}{\partial\tilde{u}}+\tilde{u}\left[-\Pi_{\rm TO}+\tfrac{1}{4}(C-2B^2)F_{\rm TA}(T)+\tfrac{3}{4}\eta^2\frac{N}{\omega_0}A\coth\frac{\omega_0}{2T}\right]=0\,. \tag{4.8}$$

Here, we have introduced the function $F_{\rm TA}(T)=2\sum_{\rm q}q^2\langle(Q_{\rm q}^a)^\dagger Q_{\rm q}^a\rangle$ which can be explicitly calculated as

$$F_{\rm TA}=\sum_{\rm q}\phi(\mathbf{q})q^2\frac{1}{qs_P}\coth\left(\frac{qs_P}{2T}\right)=\frac{6\eta^2N}{s_0^2}t(T)\,, \tag{4.9}$$

$$t(T)=\eta^2\frac{q_Ds_P}{2}\int_0^{1/\eta}dx\frac{x^3}{x^2+1}\coth\left(\frac{\eta s_Pq_D}{2T}x\right)\sim\begin{cases}T, & T\to\infty\\ \dfrac{q_Ds_P}{4}, & T\to 0\end{cases}. \tag{4.10}$$

In the self-consistent condition (3.12), the temperature-dependent averages $\langle Q_{\rm q}^\dagger Q_{\rm q}\rangle$, $\langle(Q_{\rm q}^a)^\dagger Q_{\rm q}^a\rangle$, and $\langle Q_{\rm q}^\dagger Q_{\rm q}^a\rangle$ are all neglected, since they lead to the small changes in the order parameters and anharmonic couplings. Then Eq. (3.12) is written in the form

$$\frac{\partial E_0}{\partial\tilde{\epsilon}}-\tilde{\epsilon}\Pi_{\rm TA}=0\,. \tag{4.11}$$

The self-consistency conditions (4.8) and (4.11) are rewritten conveniently as

$$\omega_P^2(T)+B\tilde{\epsilon}+\frac{A}{6}\tilde{u}^2+\frac{C}{2}\tilde{\epsilon}^2=0\,, \tag{4.12}$$
$$s_P^2\tilde{\epsilon}+\frac{B}{2}\tilde{u}^2+\frac{C}{2}\tilde{\epsilon}\tilde{u}^2=0\,, \tag{4.13}$$

where use has been made of the expression of E_0 in Eq. (3.5) as well as the soft TO-phonon frequency $\omega_P(T)$ in the cubic phase

$$\omega_P^2(T)=\omega_0^2-\Pi_{\rm TO}+\tfrac{1}{4}(C-2B^2)F_{\rm TA}(T)+\frac{3\eta^2NA}{4\omega_0}\coth\frac{\omega_0}{2T}\,. \tag{4.14}$$

The last relation is derived in Appendix B.

Let us introduce the softening temperature T_c of TO mode by

$$\omega_P^2(T_c)=0\,. \tag{4.15}$$

In the high temperature limit where T_c is larger than both the Debye frequency $\omega_D=s_Pq_D$ ($s_P^2=s_0^2-\Pi_{\rm TA}$) or the harmonic optical frequency ω_0 at the Γ point, Eq. (4.15) is solved explicitly for T_c.

$$T_c=\frac{1}{D}(\Pi_{\rm TO}-\omega_0^2)\,, \tag{4.16a}$$
$$D=\tfrac{3}{2}\eta^2N\left[\frac{1}{s_P^2}(C-2B^2)+\frac{A}{\omega_0^2}\right]. \tag{4.16b}$$

As a matter of fact, however, T_c is rather comparable to ω_D and ω_0, and Eq. (4.15) should be solved numerically. It is important to note that the coefficient D in Eq. (4.16b) depends on the electron chemical potential μ

through the acoustic-phonon self-energy Π_{TA} in the modified sound velocity s_P $[=(s_0^2-\Pi_{TA})^{1/2}]$. This means that T_c is sensitive to the change in the carrier concentration, caused by a doping or a deviation from stoichiometry. Detailed analysis of carrier concentration dependence of T_c will be given in Sec. VIII after the electron chemical potential is determined.

Now we are going to see in more detail what happens in the vicinity of T_c. To do this, it is convenient to use the following scaled quantities:

$$\tau=\frac{2C}{B^2}\omega_P^2 , \tag{4.17a}$$

$$e=-\frac{C}{B}\tilde{\epsilon} , \tag{4.17b}$$

$$\beta=2\left[\frac{s_P^2 A}{3B^2}-1\right] . \tag{4.17c}$$

Then, Eqs. (4.12) and (4.13) are combined to yield

$$\tau+e^2-2e+(2+\beta)\frac{e}{1-e}=0 , \tag{4.18}$$

which determines the static strain e as a function of reduced temperature τ, β being the material constant of the given IV-VI compound. Once e is determined from Eq. (4.18), the displacement $\tilde{u}$ is derived through Eqs. (4.13) and (4.17) in the reduced form

$$\tilde{u}^2=3\frac{B^2}{AC}\frac{e}{1-e}(2+\beta) . \tag{4.19}$$

In the limit $e\to 0$, Eq. (4.18) is read as $\tau\sim-\beta e$. This suggests that the parameter β, denoting the coupled effect of the electrostrictive coupling, TO-phonon anharmonicity, and the renormalized sound velocity of TA mode, crucially governs the nature of the phase transition. In the case of positive (negative) β we have the second- (first-) order transition, and the boundary case $\beta=0$ means that T_c becomes a tricritical point. The relations between τ and e in these cases are schematically plotted in Figs. 2(a) and 2(b). It is easy to see that the reduced strain e can move in the interval $0\le e<1$, limited by the biquadratic TA-TO phonon coupling C. For $\beta>0$, there is a metastable distorted solution $e>0$ even for the temperature $T_c<T<T_b$ (or $0<\tau<\tau_b$), in addition to the cubic solution $e=0$. The superheating temperature τ_b is derived from Eq. (4.18) as

$$\tau_b=b^2(3-2b),\quad b=1-(1+\tfrac{1}{2}\beta)^{1/3} \tag{4.20}$$

where the superheating strain is denoted by b. When the tricritical condition $\beta=0$ is met, the strain e behaves as a function of τ in the way

$$e\simeq(-\tau/3)^{1/2} , \tag{4.21}$$

in the vicinity of the transition point.

V. BEHAVIOR OF THE SOFT TO MODE NEAR THE TRANSITION POINT

As is assumed throughout the paper, the structural phase transition in the IV-VI compounds is triggered by the softening of TO phonons at the Γ point. In fact, we have shown in Appendix B that the renormalized TO-phonon frequency in the rhombohedral phase is expressed in the form

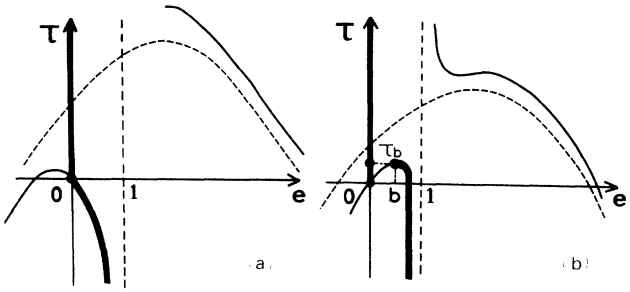

FIG. 2. The schematic representation of the reduced temperature τ versus the reduced strain e given by Eq. (4.18). The thick solid curves denotes the physical branches in cases of (a) the second-order phase transition ($\beta>0$) and (b) the first-order phase transition ($\beta<0$). b and τ_b denote the superheating reduced strain and temperature, respectively.

$$\omega_F^2=\omega_P^2+\frac{\partial^2 E_0}{\partial\tilde{u}^2}-\omega_0^2 , \tag{5.1}$$

where the first term represents the corresponding frequency in the cubic phase given in Eq. (4.14). In connection with experiments, ω_P should be identified with the frequency of the F_{1u} mode; the observed soft mode in the IV-VI compound with rock-salt structure. Similarly, ω_F corresponds to the A_1 mode. In the case of $\beta>0$, we can rewrite Eq. (5.1) in the form

$$\omega_F^2=\frac{A}{3}\tilde{u}^2\sim-\frac{B^2}{C}\left[1+\frac{2}{\beta}\right]\tau , \tag{5.2}$$

while we get

$$\omega_F^2\sim 2\frac{B^2}{C}\left[-\frac{\tau}{3}\right]^{1/2} \tag{5.3}$$

in the tricritical transition $\beta=0$. As already seen in Sec. IV, the first-order transition takes place for $\beta<0$ at the reduced temperature $\tau_b>0$, associated with a discontinuous growth of order parameters. In the vicinity of this temperature, the TO-phonon frequency (5.1) behaves as

$$\omega_F^2=\frac{\beta^2}{C}\left[b\frac{2+\beta}{1-b}+2(1-b)\left[\frac{\tau_b-\tau}{3}\right]^{1/2}\right] . \tag{5.4}$$

Summarizing these results, we show the variation of soft TO-phonon frequency with temperature schematically in Figs. 3(a)–3(c). In particular, for $\beta<0$ in the temperatures $[0,\tau_b]$, we expect a hysteresis in the process of decreasing or increasing T.

Finally let us discuss the ratio ζ of the slopes of the curves in Fig. 3, measured in the vicinity of the second-order phase transition ($\beta>0$):

$$\zeta=-\frac{d}{dT}\omega_F(A_1)^2\Big/\frac{d}{dT}\omega_P(F_{1u})^2 . \tag{5.5}$$

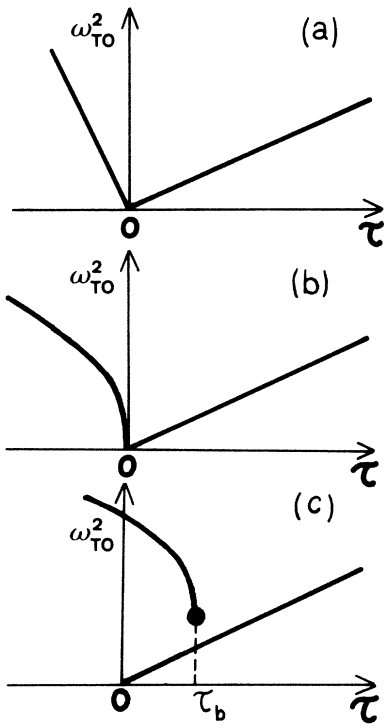

FIG. 3. The squared TO-phonon frequency for (a) $\beta>0$ (second-order phase transition), (b) $\beta=0$ (tricritical point), and (c) $\beta<0$ (first-order phase transition). The abscissa τ is a monotonic increasing function in T.

Making use of Eqs. (4.17a) and (5.2), we find the expression for this ratio

$$\zeta=2\left[1+\frac{2}{\beta}\right] . \tag{5.6}$$

In the absence of electrostrictive coupling ($\beta\rightarrow\infty$), this reproduces the famous result $\zeta=2$ in the Landau theory. As a matter of fact, the experiments by Jantsch[46] on the compounds $Pb_{1-x}Ge_xTe$ ($x=0.0056$–0.036) show a wide scattering of ζ from 3.3 up to 21, provided the frequency of A_1 mode is 3 times larger than that of the E mode.[47] This clearly suggests that the electrostrictive coupling is really playing an active role in the phase transition of these compounds. In addition, observation of surprisingly large $\zeta(\sim 20)$ may be explained as the result of vanishingly small β (meaning a strong electrostrictive coupling), since ζ becomes infinite as the tricritical point is approached.

VI. ACOUSTIC ANOMALY

As is shown in Appendix B, inclusion of the self-energy correction due to bilinear intermode coupling (3.9) leads to an additional renormalization δ of the TA-phonon velocity in the rhombohedral phase such as

$$s_F^2=(s_0'')^2-\delta , \tag{6.1}$$

where

$$\delta\simeq\frac{\tilde{u}^2}{\omega_F^2}B^2 . \tag{6.2}$$

Since the squared sound velocity is proportional to the shear elastic modulus C_{44}, δ is interpreted as a change $\Delta C_{44}=C_{44}^F-C_{44}^P=-\rho\delta$:

$$\Delta C_{44}=\frac{\tilde{u}^2}{\omega_F^2}\frac{B^2}{s_P^2} , \tag{6.3}$$

where C_{44}^P is the shear modulus in the cubic phase. It should be noted that ΔC_{44} does not vanish even in the limit $T\rightarrow T_c-0^+$ ($\beta>0$ is assumed here), since ω_F is proportional to $\tilde{u}$ near T_c. This leads to the acoustic anomaly with a discontinuous change in the sound velocity and shear modulus on crossing T_c. Making use of Eqs. (5.3) and (4.17c), we find

$$\Delta C_{44}=-\frac{2}{2+\beta}C_{44}^P , \tag{6.4}$$

in the case of second-order transition ($\beta>0$). It is clear that ΔC_{44} vanishes in the absence of the electrostrictive coupling ($\beta\rightarrow\infty$). It is also seen from this equation that the sound velocity vanishes at the tricritical point $\beta=0$. In other words, the TA mode is softened at the tricritical point. In the first-order transition, the discontinuity

$$\Delta C_{44}=\left[-1+\frac{3}{(1-b)^2}\left[\frac{\tau_b-\tau}{3}\right]^{1/2}\right]C_{44}^P , \tag{6.5}$$

is expected where b is the reduced strain at this temperature.

Let us remark on the stability of the superheated branch, i.e., $(\omega_{q-})^2\geq 0$. This condition can be related to the slope of the order parameter with respect to the temperature

$$C_{44}^F=\frac{3}{2}\rho\frac{B^2}{A}(1-e)\left[-\frac{\partial\tau}{\partial e}\right]\geq 0 , \tag{6.6}$$

which states that the TA mode is stable on the $\langle\epsilon\rangle-T$ line with a negative temperature coefficient, and the shear modulus C_{44} in the rhombohedral phase vanishes. The TA mode is softened at the superheating point in the case $\beta<0$. At this point, the derivative $\partial e/\partial\tau\propto\partial\langle\epsilon\rangle/\partial T$ becomes divergent.[48] It is also seen from Eq. (6.6) that the increasing tendency of C_{44} with lowering temperature[49] is attributed to the saturation of the order parameters. Equation (6.6) is rewritten as

$$C_{44}^F=\frac{2}{1-e}\frac{(d/dT)\omega_P^2}{(d/dT)\omega_F^2}C_{44}^P \tag{6.7a}$$

$$\simeq\frac{2}{\zeta}C_{44}^P=\frac{\beta}{2+\beta}C_{44}^P . \tag{6.7b}$$

It is to be noted that there is a definite connection between the acoustic anomaly and the deviation of the ratio ζ from 2: both are crucially governed by the electrostrictive coupling B.

VII. MODIFIED TWO-BAND ELECTRONS

We are going to discuss the effects of the structural phase transition on the electronic states in our system. As already mentioned, we have assumed that the dominant effects of the transition is expressed in terms of the self-energy correction due to static distortions $\tilde{u}=\sqrt{3NM}\langle u\rangle$ and $\tilde{\epsilon}=\sqrt{12\rho}\langle\epsilon\rangle$. The motion of electron in the distorted phase is described by a matrix Green function, given in Eq. (4.2a). Then the electronic spectrum in the distorted phase is derived from the condition $\det[\hat{G}^j(\mathbf{k},E(\mathbf{k})+i0^+)]^{-1}=0$. Solving the resulting quartic equation explicitly, we obtain the bands

$$\tilde{E}^j_{c\pm}(\mathbf{k})=\langle\epsilon\rangle\Xi^{(j)}_+ +\lambda^{(j)}_\pm(\mathbf{k}) , \tag{7.1a}$$

$$\tilde{E}^j_{v\pm}(\mathbf{k})=\langle\epsilon\rangle\Xi^{(j)}_+ -\lambda^{(j)}_\pm(\mathbf{k}) , \tag{7.1b}$$

where

$$\lambda^{(j)}_\pm(\mathbf{k})=\left[(\Delta+\langle\epsilon\rangle\Xi^{(j)}_-)^2+(\boldsymbol{\kappa}^j\cdot\hat{\mathbf{g}}^j)^2 + \left[|\boldsymbol{\kappa}^j\times\hat{\mathbf{g}}^j|\pm\sqrt{3}\frac{\langle u\rangle}{a}\Xi^{(j)}_{\rm op}\right]^2\right]^{1/2} . \tag{7.2}$$

In these expressions $\hat{\mathbf{g}}^j=\mathbf{g}^j/|\mathbf{g}^j|$, κ^j_n is a crystal momentum modified by the electron velocity matrix elements $\mathbf{W}(n)$ as defined in Eq. (2.7), and $\Xi^{(j)}_\pm$ and $\Xi^{(j)}_{\rm op}$ are the acoustic and optical deformation potentials at the jth L point, respectively (see Appendix A). The alternative signs $\pm$ indicate the Kramers pair: The degeneracy of this pair is lifted up here, reflecting the broken inversion symmetry in the rhombohedral phase with relative sublattice displacement. It is noted that the minimum band gap between the new bands depends only on $\langle\epsilon\rangle$ and not on $\langle u\rangle$. It is important to note that the original electron bands are strongly nonparabolic even in the vicinity of the L points. This is due to the spin-orbit interaction. Then we introduce an energy-dependent reciprocal effective mass tensor at the jth L point by

$$\alpha^j_{mn}=\frac{1}{k_m-k^j_m}\frac{\partial}{\partial k_n}\lambda^{(j)}_\pm(\mathbf{k}) . \tag{7.3}$$

Calculated on the Fermi surface, this yields

$$\alpha^j_{mn}(E_F)=\alpha^j_{mn}(0)\frac{\Delta}{\Delta+E_F}\left[1-\langle\epsilon\rangle\Xi^{(j)}_-\frac{\Delta}{(\Delta+E_F)^2} \pm\sqrt{3}\frac{\langle u\rangle}{a}\Xi^{(j)}_{\rm op}\frac{\Delta^2}{E_F(\Delta+E_F)^2}\right] , \tag{7.4}$$

where $\alpha^j_{mn}(0)$ means the value at the band edge from which the Fermi energy E_F is measured.

To derive variation of transition temperature T_c with the carrier concentration, we have to determine the electron chemical potential μ, formally defined by

$$N+n-p=\sum_j T\sum_n e^{i\omega_n 0^+}\sum_{\mathbf{k}}\mathrm{Tr}[\hat{G}^j(\mathbf{k};i\omega_n)] . \tag{7.5}$$

Here n and p denote the densities of conduction electrons and valence holes, respectively, and N is the density of the valence electrons in the filled valence band. The left-hand side (lhs) of Eq. (7.5) should be interpreted as the effective number of the valence electrons, including the extrinsic contributions from incomplete stoichiometry or the doped impurities.

In the absence of the extrinsic carriers at $T=0$ K (i.e., $n=p=0$ and $\mu=\Delta$), Eq. (7.5) gives

$$N=\tfrac{8}{3}\Omega\kappa_0^3=\frac{4}{3\pi^2}\frac{\kappa_0^3}{\mathbf{W}(1)\times\mathbf{W}(2)\cdot\mathbf{W}(3)} , \tag{7.6}$$

where $\mathbf{W}(n)$ ($n=1$, 2, and 3) are the interband matrix elements of velocity operators [see Eq. (2.8)], and κ_0 is the half width of symmetric bands in the space of the modified crystal momentum. Making use of the expressions for these elements, we see that

$$\kappa_0=\frac{\pi}{a}(v_\parallel v_\perp^2)^{1/3} , \tag{7.7}$$

where $N=4\pi/(3a^3)$ and a is the lattice constant.

Since the observed T_c in IV-VI compounds is always an order of magnitude smaller than the band gap 2Δ, it is safely assumed that the electrons are completely Fermi degenerate.[2] In this limit, the r.h.s. of Eq. (7.5) is calculated to yield

$$\mu=\mathrm{sgn}(n-p)\left[\Delta^2+\kappa_0^2\left[\frac{n-p}{N}\right]^{2/3}-8\frac{\langle u\rangle^2}{a^2}(\Xi_{\rm op})^2\right]^{1/2} . \tag{7.8}$$

It is seen that μ is independent of $\langle\epsilon\rangle$, since no volume change is associated with the shear strain in the lowest order of $\langle\epsilon\rangle$.

It is interesting to see that μ decreases with increases in $\langle u\rangle$, while the opposite is the case in the usual vibronic theory[2,3,8,31] based on the isotropic two-band model without spin-orbit coupling. This suggests that the distortion of Fermi surface takes place quite differently in these two models.[9,26] In the rhombohedral phase in our model, originally degenerate Kramas doublet α and β are split in a plane of $\boldsymbol{\kappa}$ normal to the vector $\mathbf{g}^j$ whose components stand for the coupling constants of different channels of electron–TO-phonon scattering. Let us denote by $\kappa_\perp$, the radius of a cross section of Fermi surface (specified by a fixed $\kappa_\parallel$). As $\langle u\rangle$ appears, this radius changes its value from $\kappa_\perp$ to $\kappa_\perp+\delta\kappa_\perp$, $\delta\kappa_\perp$ being proportional to $\langle u\rangle$. This results in an increase in the available phase volume by the amount $2\pi\delta\kappa_\perp^2$, leading to a decrease in μ.

Finally we show the explicit forms of the modified band-edge structures. The four equivalent valleys at the L points (D_{3d}) split into a singlet T valley (C_s) and three equivalent L valleys (C_{3v}) with a lift of the Kramers degeneracy except for on the T and L points. The Fermi surfaces are distorted from ellipsoids of revolution and carrier redistribution occurs among these nonequivalent

valleys.[9,26] For a singlet valley, Eq. (7.2) becomes

$$\lambda_{\pm}^{(1)}(\mathbf{k})=\{(\Delta+\langle\epsilon\rangle\Xi_{-}^{(1)})^2 +[v_{\perp}(k_x^2+k_y^2)^{1/2}\pm\frac{\langle u\rangle}{a}\Xi_{\rm op}^{(1)}]^2+v_{\parallel}^2k_z^2\}^{1/2}\ , \tag{7.9}$$

where the x, y, and z axes are taken in the $[\bar{1}\,\bar{1}\,2]$, $[1\bar{1}0]$ and $[111]$ directions, respectively. The upper state has a smaller volume and strong mass anisotropy. The down state has a larger volume, and the Fermi surface is significantly distorted to a form like an elongated apple. For the triplet valley, on the other hand, the electron spectrum becomes more complicated as

$$\lambda_{\pm}^{(2)}(\mathbf{k})=\left[(\Delta+\langle\epsilon\rangle\Xi_{-}^{(2)})^2+\left[\frac{\langle u\rangle}{a}\Xi_{\rm op}^{(2)}\right]^2 +v_{\perp}^2(k_x^2+k_y^2)+v_{\parallel}^2k_z^2\pm\tfrac{2}{3}\frac{\langle u\rangle}{a}[(\Xi_{\parallel}v_{\perp}k_x+2\sqrt{2}\Xi_{\perp}v_{\parallel}k_z)^2+(3\Xi_{\rm op}^{(2)}v_{\perp}k_y)^2]^{1/2}\right]^{1/2}\ , \tag{7.10}$$

where x, y, and z axes are in the directions $[112]$, $[\bar{1}10]$, and $[\bar{1}\,\bar{1}\,1]$, and $\Xi_{\rm op}^{(1)}$ and $\Xi_{\rm op}^{(2)}$ are defined by

$$\Xi_{\rm op}^{(1)}=\Xi_{\parallel}\ , \tag{7.11a}$$

$$\Xi_{\rm op}^{(2)}=\Xi_{\rm op}^{(3)}=\Xi_{\rm op}^{(4)}=\tfrac{1}{3}(\Xi_{\parallel}^2+8\Xi_{\perp}^2)^{1/2}\ . \tag{7.11b}$$

The last relations are derived from Eq. (A6) and Table VI. The upper state has a smaller volume and stronger mass anisotropy, while the down state has a larger volume with a smaller distortion from the revoluted ellipsoid. These complicated Fermi surfaces have been used by Murase[26] and Takaoka[9] to interpret a knotty oscillation in the Schubunikov–de Haas coefficients in the IV-VI compounds.

VIII. COMPARISON WITH EXPERIMENTS

In this section we try to interpret the experimental results in SnTe or other IV-VI compounds, and further predict the unobserved quantities in SnTe such as the jump of shear modulus ΔC_{44}, the temperature derivative of the squared TO-phonon frequency in the cubic phase $d\omega_P^2/dT$, the ratio of the temperature derivatives of squared TO-phonon frequencies ζ, and the combination of phonon coupling constants β.

At first, we list the experimental data for SnTe in Table I, used to determine the fitting parameters in our theory. As shown in the experiments of the shear modulus [(1) of Table I] and the critical temperatures (Fig. 4), the prominent dependence of carrier concentration is seen in SnTe. Unfortunately the other experimental data listed in Table I are obtained for different carrier concentrations. Thus we have to carefully estimate the values of many fitting parameters in our model so as to reproduce the various experimental results with different carrier concentrations. First of all, we show in Table II the parameters whose values are considered to be rather well established. Making use of these values of parameters, we have fitted the experiments in Table I and the resultant fitted parameters are summarized in Table III, although some ambiguities are present as discussed below. The theoretical T_c-p curve is shown in Fig. 4 in which the theoretical curve has been adjusted to the data of Iizumi *et al.*[50] with $p=0.88\times10^{20}$ cm^{-3}. The theory can reproduce the experimental data well. The dotted (dashed) curve represents the result obtained by taking account of the effect of polarization only of the TA (TO) mode. Comparing these results, we see that the contributions from both modes are comparatively important. In Fig. 5, we show the calculated $\langle u\rangle-T$ curve at the hole concentration $p=0.88\times10^{20}$ cm^{-3}, together with the experimental data measured by Iizumi *et al.*[50] As the temperature is lowered, the calculated curve deviates upward systemati-

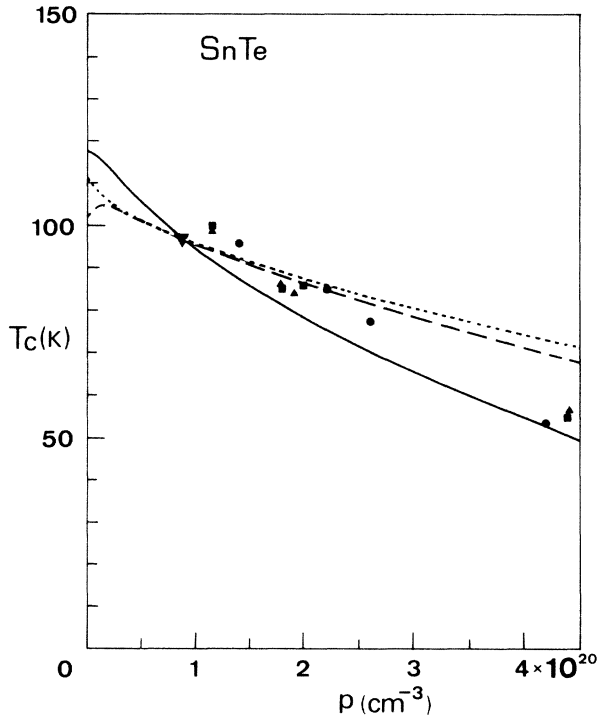

FIG. 4. Carrier concentration dependence of the transition temperature T_c in SnTe. The abscissa denotes the hole concentration p. The solid curve denotes the softening temperature of TO mode calculated by Eq. (4.14). The dotted (dashed) curve denotes the theoretical result obtained by taking account of the effect of polarization only of the TA (TO) mode. The experimental data are from (●) Sugai *et al.* (Ref. 68), (▲) Murase and Nishi (Ref. 28), (■) Kobayashi *et al.* (Ref. 27), and (▼) Iizumi *et al.* (Ref. 50). Three theoretical curves are adjusted to the data of Iizumi *et al.* with $p=0.88\times10^{20}$ cm^{-3}.

TABLE I. Experimental data in SnTe

Quantity		Value	Hole concentration p ($\times 10^{20}$ cm^{-3})
(1) Shear modulus	C_{44}^{P} ($T=293$ K)	1.235×10^{11} dyn cm^{-2}	1.01
in cubic phase[a]		0.969×10^{11} dyn cm^{-2}	4.50
(2) Average band gap[b]	$d\tilde{E}_G^{\rm av}/dT$ ($T<T_c$)	-0.25 meV/K	1.3
	$dE_G^{\rm av}/dT$ ($T>T_c$)	0.15 meV/K	1.3
	$E_G^{\rm av}$ ($T=T_c$)	2.0 eV	1.3
(3) Temperature derivatives of squared TO-phonon frequency in rhombohedral phase[c]	$\frac{d}{dT}\left[\frac{\omega_F}{2\pi c}\right]^2$ (A_1 mode)	-23.15 cm^{-2}/K	1.4
(4) Jump of specific heat[d]	Δc_p	0.457 J mol^{-1}K^{-1}	1.8
(5) Critical temperatures	$T_c(p)$	Fig. 4	1.16–4.42
(6) Static sublattice	$\langle u\rangle(T)$	Fig. 5	0.88
displacement[e]	$\frac{d}{dT}\frac{\langle u\rangle^2}{a^2}$	-0.154 K^{-1}	0.88

[a]Seddon and Gupta (Ref. 29).
[b]K. Murase and S. Sugai, Solid State Commun. **32**, 89 (1979).
[c]Murase and Sugai, Solid State Commun. **32**, 89 (1979); cited by Jantsch (Ref. 5, Table 5.1).
[d]I. Hatta and K. L. I. Kobayashi, Solid State Commun. **22**, 775 (1977).
[e]Iizumi *et al.* (Ref. 50).

cally. Making use of the parameters in Tables II and III, we calculate various physical quantities as summarized in Table IV. Comparing Tables I and IV, it is shown that satisfactory agreements between theory and experiments are obtained. Although there is no experimental data of $d\omega_P^2/dT$, our theory predicts the rather small value of β which is responsible for the larger ζ than the previous mean-field value 2 as discussed in Sec. V. To confirm our prediction, a systematic measurement of squared TO-phonon frequency in the cubic phase (ω_P^2) at various temperatures near T_c is strongly desired. The application of hyper Raman scattering[51] will be promising for this purpose.

We note here some ambiguities in the choice of the fitting parameters in Table III. At first, the acoustic deformation potentials are tentatively chosen in Table III, taking account of the calculated values in SnTe [$\Xi(L_{61}^{-})=7.98$ eV, $\Xi(L_{61}^{+})=7.35$ eV] (Ref. 52) and PbTe [$\Xi(L_{61}^{-}=8.3$ eV, $\Xi(L_{61}^{+})=10.5$ eV] (Ref. 53). This will be improved when much data are measured for the shear modulus C_{44}^{P} in the cubic phase at least for three different hole concentrations. Second, the biquadratic coupling C

TABLE II. Values of physical parameters in SnTe.

Velocity matrix elements[a]	$v_{\parallel}$	2.4×10^{7} cm sec^{-1}
	$v_{\perp}$	7.9×10^{7} cm sec^{-1}
Half band gap at L point[b]	$\Delta(T)=-181.8+[40.96+0.0475(T+20)^2]^{1/2}$ meV	
Density[c]	ρ	6.383 g cm^{-3}
Lattice constant[c]	a	6.327×10^{-8} cm
Reduced mass in a unit cell[d]	M	1.31×10^{-22} g

[a]The velocity matrix elements are evaluated by the relation $v_{\perp,\parallel}^2=(2P_{t,l}^2/m_0)/(2m_0)$, where $2P_t^2/m_0=7.1$ eV and $2P_l^2/m_0=0.68$ eV have been used (Ref. 4, p. 49).
[b]Nimtz and Schlicht (Ref. 4, Sec. 3.2.3.1).
[c]Nimtz and Schlicht (Ref. 4, Table 2. 3).
[d]V. L. Volkov, Fiz. Tekh. Poluprovodn. **12**, 396 (1978) [Sov. Phys.—Semicond. **12**, 229 (1978)].

TABLE III. Values of fitted parameters in SnTe. These values are determined by the experimental data listed in Table I indicated in the right most column.

Quantity		Value	Table I reference
Bare TO-phonon frequency	ω_0	1.2 THz	(5),(6)
Cutoff parameter	η	0.024	(5),(6)
Acoustic deformation potentials	$\Xi(L_{61}^{-})$	10.4 eV	(1)
	$\Xi(L_{61}^{+})$	9.77 eV	(1)
Bare shear modulus	C_{44}^{0}	1.40×10^{11} dyn cm^{-2}	(1)
Optical deformation potential	$\Xi_{\rm op}$	9.3 eV	(2)[a]
Quartic coupling of TO phonon	$\bar{A}=(3NM)^2A$	1.05×10^{45} erg cm^{-7}	(3),(6)
Electrostrictive coupling between TA and TO phonons	$\bar{B}=\sqrt{12\rho}3NMB$	-1.71×10^{28} erg cm^{-5}	(3),(4),[b](6)
Biquadratic coupling between TA and TO phonons	$\bar{C}=12\rho3NMC$	4.16×10^{32} erg cm^{-5}	(5)

[a]To determine the optical deformation potential $\Xi_{\rm op}$, we have used $\tilde{E}_G^{\rm av}=E_G^{\rm av}+6(\langle u\rangle/a)^2\Xi_{\rm op}^2/E_G^{\rm av}$, where $\tilde{E}_G^{\rm av}$ is defined by (Ref. 3) $(\tilde{E}_G^{\rm av})^2=\sum_{\mathbf{k}}\sum_{j\pm}[\tilde{E}_{c\pm}^{j}(\mathbf{k})-\tilde{E}_{v\pm}^{j}(\mathbf{k})]^2/\sum_{\mathbf{k}}\sum_{j\pm}$.

[b]The jump of the specific heat ΔC_p is used to determine $d\omega_P^2/dT$ through the relation (Ref. 12) $\Delta C_p=-(3NM/2)T_c(d\langle u\rangle^2/dT)(d\omega_P^2/dT)$.

cannot uniquely be determined, because of a lack of the experimental values of static rhombohedral shear strain $\langle\epsilon\rangle$ in the bulk sample. When the data of $\langle\epsilon\rangle$ are obtained as a function of the temperature, we can determine C because the ratio C/A affects the magnitude of $\langle\epsilon\rangle$. Although $\langle\epsilon\rangle$ is measured by Muldawer,[54] his data is in contradiction with the experimental second-ordered phase transition in SnTe:[50] If we adopt the data by Muldawer, the electrostrictive coupling B becomes too strong to give negative β, and the first-order phase transition is predicted. We may attribute this discrepancy to the fact that the powder sample is used by Muldawer; a larger macroscopic displacement of crystal lattice is needed in bulk than in powder to grow the rhombohedral shear.

Finally we discuss the experimental results of IV-VI compounds other than SnTe. Let us first compare the fitted parameters and calculated physical quantities in SnTe with that in $Pb_{1-x}Ge_xTe$. The experimental data and resultant parameters are listed in Table V. The phonon coupling constants A and B are shown to be comparable to those in SnTe (Table III). It is also seen that the estimated value of β in SnTe is smaller than that in $Pb_{1-x}Ge_xTe$. This is reflected in a larger ζ and ΔC_{44} in SnTe. The vanishingly small β is, on the other hand, realized in $Ge_{1-x}Sn_xTe$ ($x=0.72$) (Ref. 15) at which the tricritical point takes place and ζ would be infinitely large. It is also known in $Pb_{1-x}Sn_xTe$ that the critical temperature becomes independent of the carrier concentration as the composition x decreases.[27,28] This may be attributed to an increase in the bare harmonic frequency of the TO mode ω_0, and/or A/C with a decrease in x. The former is responsible for the effective reduction of the carrier concentration dependence in $\Pi_{\rm TO}$, and the latter for that in $\Pi_{\rm TA}$.

IX. DISCUSSION

We saw in Sec. VIII that the shear modulus C_{44} decreases monotonically as a function of the free carrier concentration. This is physically interpreted as follows. First of all, we note that a single-band free electron gas cannot affect the shear modulus and sound velocity, because shear strain involves no volume change.[55] Thus the

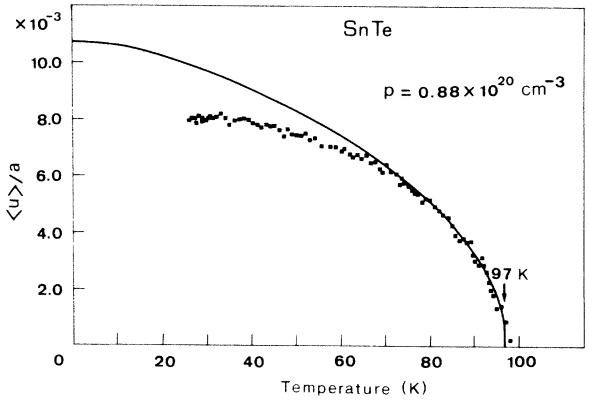

FIG. 5. Relative sublattice displacement $\langle u\rangle/a$ versus temperature in SnTe with hole concentration $p=088\times10^{20}$ cm^{-3}. The solid curve is calculated from Eqs. (4.12) and (4.13). The solid squares are the experimental data of Iizumi *et al.* (Ref. 50). The arrow indicates the calculated transition temperature $T_c=97$ K.

TABLE IV. Calculated physical quantities in SnTe at the transition point.

Quantity		Value	Hole Concentration p ($\times 10^{20}$ cm^{-3})
Critical temperature	T_c	94.6—45.3 K	1—5
Shear modulus in cubic phase	C_{44}^P	$1.21-0.88\times 10^{11}$ dyn cm^{-2}	1—5
Jump of shear modulus	ΔC_{44}	$0.694-0.694\times 10^{11}$ dyn cm^{-2}	1—5
Temperature derivatives of squared TO-phonon frequencies	$\frac{d}{dT}\left[\frac{\omega_F}{2\pi c}\right]^2$	$-21.31--55.84$ -23.18	1—5 1.4
	$\frac{d}{dT}\left[\frac{\omega_P}{2\pi c}\right]^2$	4.55—5.86 4.70	1—5 1.4
Jump of specific heat[a]	ΔC_p	1.058 J mol^{-1} K^{-1}	1.8
Temperature derivative of squared sublattice displacement	$\frac{d}{dT}\frac{\langle u\rangle^2}{a^2}$	-0.154 K^{-1}	0.88
Ratio of temperature derivatives of squared TO-phonon frequencies	ζ	4.69—9.53	1—5
Combination of phonon coupling constants	β	1.49—0.53	1—5

[a]The jump of specific heat is evaluated by the equation given in footnote b of Table III.

multiple-valley structure of the electron bands in the IV-VI compounds is essential to interpret this effect. In fact, the rhombohedral shear is accompanied with a deformation potential which can split the degenerate valleys at the four equivalent L points into a siglet T valley and a set of triplet L valleys,[56] just as in bismuth and antimony. Associated with the change in the valley energies is a redistribution of electrons to minimize their free energy in the strained crystal. Some amount of work done to strain the crystal will be relaxed in the course of this redistribution, resulting in a smaller effective elastic constant. The effect will be enhanced for higher carrier concentration (or equivalently for large Fermi energy). Furthermore, it should be stressed that the effect is further enhanced by the nonparabolic nature of the bands in the unstrained crystal due to strong spin-orbit coupling.[57,58]

The momentum cutoff in Eq. (4.6) is introduced to remove the following contradiction. We note that the coupling constant A can be estimated in two ways. The first is to make use of the experimental data of $\partial\omega_F^2/\partial T$, combined with Eqs. (5.5) and (4.14), assuming that $\zeta>2$ and $\omega_0^2-\Pi_{\rm TO}<0$. Another method is to combine the experimental data of $\partial\omega_F^2/\partial T$ and $\partial\langle u\rangle^2/\partial T$ with Eq. (5.2). The result of our analysis without momentum dependence of A shows that the value of A, estimated by the former method, is always larger than the second.

Throughout the paper, we have assumed that the effect of the vibronic anharmonicity[2] is always small compared with that of the lattice anharmonicity. This is explicitly confirmed in Appendix C, where it is shown that the vibronic contribution to the TO-phonon self-energy, calculated in the fourth order with respect to electron—TO-phonon interaction, is always negative in the presence of the spin-orbit coupling. This means that the parameter β is always negative, and softening transition of the TO mode becomes the first order if the vibronic anharmonicity is playing the dominant roles. This is clearly not the case in the real system such as in SnTe where the second-order transition is observed.[50] We have neglected the self-energy insertions and vertex corrections to the electron Green functions due to TA and TO phonons, based on a similar consideration.

Finally let us discuss the roles of the long-wavelength fluctuations to determine the eigenfrequencies of the coupled phonon system. If the fluctuations are completely neglected, these eigenfrequencies can be calculated as the curvatures at the minimum of the phenomenological Landau free energy F along the principal axis in the $\tilde{\epsilon}$-$\tilde{u}$ plane. Here F is formally given by replacing ω_0 and s_0 by $\omega_P(T,\mu)$ and $s_P(\mu)$, respectively, in Eq. (3.5). Such an idea leads to the expressions of eigenfrequencies of the form

$$\omega_{\pm}^2=\frac{1}{2}\left\{\frac{\partial^2 F}{\partial\tilde{u}^2}+\frac{\partial^2 F}{\partial\tilde{\epsilon}^2}\pm\left[\left[\frac{\partial^2 F}{\partial\tilde{u}^2}-\frac{\partial^2 F}{\partial\tilde{\epsilon}^2}\right]^2+4\left[\frac{\partial^2 F}{\partial\tilde{u}\partial\tilde{\epsilon}}\right]^2\right]^{1/2}\right\}. \tag{9.1}$$

TABLE V. Experimental data (1)–(5) and calculated parameters (6)–(10) at the transition point in $Pb_{1-x}Ge_xTe$. The right most column in (6)–(10) indicates the experimental data used to determine the parameters (6)–(10).

Quantity		Value	Table V reference
(1) Shear modulus in cubic phase[a]	C_{44}^P	1.35×10^{11} dyn cm^{-2}	
(2) Jump of shear modulus[a]	ΔC_{44}	0.26×10^{11} dyn cm^{-2}	
(3) Temperature derivative of squared TO-phonon frequency in rhombohedral phase[a]	$\frac{d}{dT}\left[\frac{\omega_F}{2\pi c}\right]^2$ (A_1 mode)	-15.0 cm^{-2}/K	
(4) Temperature derivative of shear distortion[b]	$\frac{d}{dT}\langle\epsilon\rangle$	-1.50×10^{-5} K^{-1}	
(5) Temperature derivative of squared sublattice displacement[c]	$\frac{d}{dT}\frac{\langle u\rangle^2}{a^2}$	-4.60×10^{-7} K^{-1}	
(6) Ratio of temperature derivatives of squared TO-phonon frequencies	ζ	2.48	(1),(2)
(7) Combination of phonon coupling constants	β	8.38	(1),(2)
(8) Jump of specific heat	ΔC_p	0.239J mol^{-1}K^{-1}	(3),(5),(6)
(9) Quartic coupling of TO phonon	$\bar{A}$	4.9×10^{45} erg cm^{-7}	(3),(5)
(10) Electrostrictive coupling between TA and TO Phonons	$\bar{B}$	-2.0×10^{28} erg cm^{-5}	(4),(5)

[a]Sugai *et al.* (Ref. 49).
[b]D. K. Hohnke, H. Holloway, and S. Kaiser, J. Phys. Chem. Solid **33**, 2053 (1972).
[c]Calculated values by Sugai *et al.* (Ref. 49).

If we assume $\partial^2F/\partial\tilde{u}^2 \gg \partial^2F/\partial\tilde{\epsilon}^2$, then the frequency

$$\omega_-^2=\frac{\partial^2F}{\partial\tilde{\epsilon}^2}-\frac{\partial^2F}{\partial\tilde{\epsilon}\partial\tilde{u}}\left[\frac{\partial^2F}{\partial\tilde{u}^2}\right]^{-1}\frac{\partial^2F}{\partial\tilde{u}\partial\tilde{\epsilon}}\ , \tag{9.2}$$

is obtained for the modified acoustic mode. This is equivalent with Eqs. (B14)–(B16). It should be noted that the condition $\partial^2F/\partial\tilde{u}^2 \gg \partial^2F/\partial\tilde{\epsilon}^2$ does not hold, because $\partial^2F/\partial\tilde{u}^2\sim\omega_P^2\sim0$ and $\partial^2F/\partial\tilde{\epsilon}^2\sim s_P^2$ near the transition point at which the acoustic anomaly takes place. Slonszewski and Thomas[12] derived the above expression by calculating $d^2F/d\tilde{\epsilon}^2$ along the line of $\tilde{u}=\tilde{u}(\tilde{\epsilon})$ specified by $\partial F/\partial\tilde{u}=0$, on the assumption that the optical vibration is far more rapid than the acoustic motion. As is clear from the above discussion, their assumption is not satisfied in the context of the Landau theory. However, this assumption should be interpreted as $\omega_P^2 \gg q^2s_P^2$ rather than $\partial^2F/\partial\tilde{u}^2 \gg \partial^2F/\partial\tilde{\epsilon}^2$. The former inequality holds well in the long-wavelength limit even near the transition point. This is in harmony with our basic standpoint such that all physical quantities are considered in the long-wavelength limit.

Although the Landau free energy F has no dynamical significance, $F=F(\tilde{u},\tilde{\epsilon}(\tilde{u}))$ is meaningful for finding the equilibrium configuration.[12] The order parameter $\tilde{u}$ is then determined by

$$\frac{1}{\tilde{u}}\frac{\partial F}{\partial\tilde{u}}=\omega_P^2+\beta\frac{B^2\tilde{u}^2}{4s_P^2}+\tfrac{3}{8}CB^2\frac{\tilde{u}^4}{s_P^4}\ , \tag{9.3}$$

where β is defined by Eq. (4.17c). This is an alternative form of the self-consistent condition (4.18) with small order parameters. It is thus naturally understood that the nature of the phase transition is governed by the sign of β as discussed in Sec. IV.

ACKNOWLEDGMENTS

The author is indebted to Professor Hidetoshi Fukuyama for the early stages of this work. The author would like to acknowledge the helpful suggestions of Professor Kazuo Murase, and the continuing encouragement and a critical reading of the manuscript of Professor Chikara Ishii. We also thank Dr. Akira Suzuki for stimulating and helpful discussions, and Dr. Kazuhisa Kaneda and Dr. Kazuyuki Watanabe for useful discussions.

APPENDIX A: OPTICAL AND ACOUSTIC DEFORMATION POTENTIALS

In this Appendix, we briefly summarize the definitions and properties of the matrix elements of electron velocity and optic (acoustic) deformation potential with respect to the band-edge wave functions.[59,60]

First of all, we show the band-edge states derived by Mitchel and Wallis[24] who diagonalize the six band-edge states coupled by spin-orbit coupling:

$$\phi_{c\mathbf{k}^1\beta}=|L_{61}^{-}\beta\rangle$$
$$=(\cos\theta^{-})|Z\downarrow\rangle+(\sin\theta^{-})|X_{-}\uparrow\rangle\ , \tag{A1a}$$

$$\phi_{v\mathbf{k}^1\beta}=|L_{61}^{+}\beta\rangle$$
$$=-(\cos\theta^{+})|R\downarrow\rangle+i(\sin\theta^{+})|S_{-}\uparrow\rangle\ , \tag{A1b}$$

$$\phi_{l\mathbf{k}^1\alpha}=KI\phi_{l\mathbf{k}^1\beta}\ . \tag{A1c}$$

Here $K=-i\sigma_y K_0$ and I stand for the time reversal and inversion operators, respectively. Further details of notations are to be referred to Ref. 24. To express the single electron Hamiltonian in the Dirac form, it is convenient to shift the phase of state $|L_{61}^{+}\beta\rangle$ by $\pi/2$ from the original form given in the Ref. 24. The state L_{61}^{-} (L_{61}^{+}) should be assigned as the band-edge state of conduction (valence) electron, except for the case of SnTe in which the above assignments should be reversed.[61]

Making use of these states, the matrix elements of electron velocity are calculated with the z axis along the [111] direction from the definition (2.8). This yields

$$\mathbf{W}^1(1)=(v_{\perp},0,0)\ , \tag{A2a}$$

$$\mathbf{W}^1(2)=(0,v_{\perp},0)\ , \tag{A2b}$$

$$\mathbf{W}^1(3)=(0,0,v_{\parallel})\ , \tag{A2c}$$

where $v_{\parallel}$ and $v_{\perp}$ are introduced by

$$v_{\parallel}=i\langle L_{61}^{-}\beta|\pi_z|L_{61}^{+}\beta\rangle\ , \tag{A3a}$$

and

$$v_{\perp}=-i\tfrac{1}{2}\langle L_{61}^{-}\beta|\pi_x-i\pi_y|L_{61}^{+}\alpha\rangle\ . \tag{A3b}$$

It is shown that vectors $\mathbf{W}(1)$, $\mathbf{W}(2)$, and $\mathbf{W}(3)$ are transformed similar to $[\bar{1}\,\bar{1}\,2]$, $[1\bar{1}0]$, and [111], respectively.

In a similar manner, we can calculate the elements of the optic deformation potential in the form as shown in Table VI. Here we have introduced $\Xi_{\parallel}$ and $\Xi_{\perp}$ by

$$\Xi_{\parallel}=-a\left\langle L_{61}^{-}\beta\left|\frac{\partial}{\partial z}V_p\right|L_{61}^{+}\beta\right\rangle\ , \tag{A4a}$$

and

$$\Xi_{\perp}=\tfrac{1}{2}a\left\langle L_{61}^{-}\beta\left|\frac{\partial}{\partial x}V_p-i\frac{\partial}{\partial y}V_p\right|L_{61}^{+}\alpha\right\rangle\ . \tag{A4b}$$

Combining these elements, we can define $\Xi_{\rm op}$ and $\Xi_{\rm op}^{(j)}$ by

TABLE VI. The matrix elements of optic deformation potentials $\mathbf{e}(0)\cdot\Xi^j(n)$ at the j th L point.

	$n=1$	2	3
$j=1$	0	0	$\Xi_{\parallel}$
2	$(2\sqrt{2}/3)\Xi_{\perp}$	0	$-\frac{1}{3}\Xi_{\parallel}$
3	$-(\sqrt{2}/3)\Xi_{\perp}$	$(\sqrt{6}/3)\Xi_{\perp}$	$-\frac{1}{3}\Xi_{\parallel}$
4	$-(\sqrt{2}/3)\Xi_{\perp}$	$-(\sqrt{6}/3)\Xi_{\perp}$	$-\frac{1}{3}\Xi_{\parallel}$

$$\Xi_{\rm op}=\left[\tfrac{1}{4}\sum_{j=1}^{4}(\Xi_{\rm op}^{(j)})^2\right]^{1/2}\ . \tag{A5}$$

$$\Xi_{\rm op}^{(j)}=\left[\sum_{n=1}^{3}[\mathbf{e}(0)\cdot\Xi^j(n)]^2\right]^{1/2}\ . \tag{A6}$$

The acoustic deformation potential has only intraband elements of the form

$$\Xi_{nm}^{lj}=\langle\phi_{l\mathbf{k}j_\sigma}|\delta V_{nm}(r)|\phi_{l\mathbf{k}j_\sigma}\rangle\ , \tag{A7}$$

where $\delta V_{nm}(\mathbf{r})$ is related to the local energy change due to shear strain by $\sum_{n,m}\epsilon_{nm}(\mathbf{r})\delta V_{nm}(\mathbf{r})$. The terms with $n=m$ vanish for the rhombohedral shear strain. Let us define Ξ^{lj} ($l=c$, v, and $j=1,\ldots,4$) by

$$\Xi^{lj}=\Xi_{xy}^{lj}+\Xi_{yz}^{lj}+\Xi_{zx}^{lj}\ . \tag{A8}$$

Since the shear strain involves no volume change in the first order, we have a symmetry relation between the elements Ξ^{lj} in Eq. (A8):

$$\Xi^{12}=\Xi^{13}=\Xi^{14}=-\Xi^{l1}/3\ . \tag{A9}$$

Thus the acoustic deformation potential has only two independent elements; Ξ^{c1} and Ξ^{v1} are chosen as such elements. In Sec. VIII the $\Xi^{c1}(\Xi^{v1})$ is referred to $\Xi(L_{61}^{-})$ [$\Xi(L_{61}^{+})$] to avoid the ambiguity of the assignments of the band-edge states. The electron–TA-phonon interaction can be rearranged in the matrix form as in Eq. (2.20) in the text, and the quantity $\hat{f}^j(q)$ is shown to have an expression

$$\hat{f}^j(\mathbf{q})=\frac{q}{(2qs_0)^{1/2}}\hat{\tilde{f}}^j(0)\ , \tag{A10}$$

where

$$\hat{\tilde{f}}^j(0)=\frac{1}{\sqrt{12\rho}}(\Xi_{+}^{(j)}\cdot\mathbb{1}+\Xi_{-}^{(j)}\hat{\gamma}_0)\ , \tag{A11}$$

and

$$\Xi_{\pm}^{(j)}=\Xi^{cj}\pm\Xi^{vj}\ . \tag{A12}$$

It should be noted that the $\mathbf{k}\cdot\mathbf{p}$ perturbational treatment has a special advantage to relate the band deformation potential[62] to the electron-phonon deformation potential.[63] These two coincide with each other only at the band edges.[63]

APPENDIX B: COUPLED PHONONS IN RHOMBOHEDRAL PHASE

We are going to calculate the phonon Green functions in rhombohedral phase with a special stress on the acoustic anomaly. As shown in the text, this anomaly is induced by the electrostrictive coupling of the TA mode to TO mode in the presence of order parameter $\langle u \rangle$.[12,13] In particular, it is noted that this coupling should be treated in a nonperturbative fashion taking account of the long-wavelength fluctuations of the TA mode get the anomaly.[13]

Therefore, we first calculate the TA- and TO-phonon Green functions $D''_{\rm TA}$ and $D''_{\rm TO}$ in the absence of the intermode coupling. After that, the effects of the mode coupling will be included through the Dyson equations to obtain the Green function $D_{\rm TA}$ and $D_{\rm TO}$ for the coupled phonon system.

The Green function of the TA phonon $D''_{\rm TA}$ is calculated, taking account of the processes as shown in Figs. 6(c) and 6(d). Only the particle-hole pair polarization is included, and minor temperature-dependent corrections from lattice anharmonicities are neglected, since the TA mode is not directly responsible for the transition. Thus, we obtain $D''_{\rm TA}$ of the form

$$D''_{\rm TA}(\mathbf{q};i\zeta_l)=\frac{1}{D'_{\rm TA}(\mathbf{q};i\zeta_l)^{-1}-\Pi'_{\rm TA}(\mathbf{q};i\zeta_l)}$$

$$=\frac{2qs'_0}{\zeta_l^2+q^2(s''_{\rm q})^2}\ , \tag{B1}$$

where the unperturbed Green function $D'_{\rm TA}$ and polarization $\Pi'_{\rm TA}$ are given by

$$D'_{\rm TA}(\mathbf{q};i\zeta_l)=\frac{2qs'_0}{\zeta_l^2+q^2(s'_0)^2}\ , \tag{B2}$$

$$\Pi'_{\rm TA}(\mathbf{q};i\zeta_l)=\frac{q^2}{2qs'_0}\Pi_{\rm TA}(\mathbf{q};i\zeta_l)\ , \tag{B3}$$

$$\Pi_{\rm TA}(\mathbf{q};i\zeta_l)=-\sum_{j,k}T\sum_n {\rm Tr}[\hat{\bar{f}}^j(-\mathbf{q})\hat{G}^j_0(\mathbf{k};i\omega_n)\hat{\bar{f}}^j(\mathbf{p})\times\hat{G}^j_0(\mathbf{k}-\mathbf{q};i\omega_n-i\zeta_l)]\ . \tag{B4}$$

In these expressions, the subscript 0 means the quantities in the cubic phase, and the renormalized sound velocity s''_0 is defined by

$$(s''_0)^2=(s'_0)^2-\Pi_{\rm TA}(0;i0^+)$$

$$=\frac{C^P_{44}}{\rho}+\frac{\tilde{u}^2}{2}C\ . \tag{B5}$$

In deriving the second equality of (B1), we have neglected a small term of the order ω_0/Δ. The shear modulus C^P_{44} in the cubic phase is defined from (B5) as

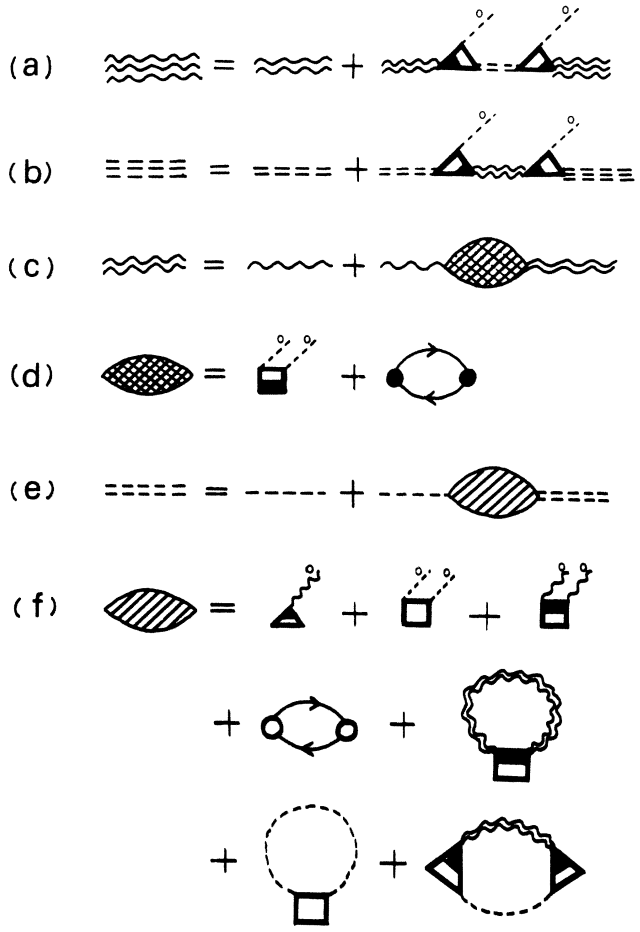

FIG. 6. Diagrammatical representations of phonon Green functions for (a) TA and (b) TO modes in ferroelectric phase. Phonon Green functions for (c) TA mode [(d) self-energy] and (e) TO mode [(f) self-energy] in the absence of mode coupling. The solid and open circles denote electron TA and TO couplings, respectively, the open square is the fourth-order anharmonicity of the TO mode A, the corner-shaded triangle is the electrostrictive coupling B, and the half-shaded square is the biquadratic coupling C. The solid line denotes the electron Green function with spin-orbit coupling. The single wavy and broken lines denote the bare TA and TO phonons, and those with superscript 0 denote order parameters $\langle \epsilon \rangle$ and $\langle u \rangle$, respectively.

$$C^P_{44}(\mu)=C^0_{44}-\frac{1}{18\pi^2 v_{\parallel}v_{\perp}^2}\times\left\{[2(\Xi^{(1)}_+)^2+(\Xi^{(1)}_-)^2]\,|\mu|\,(\mu^2-\Delta^2)^{1/2}-(\Xi^{(1)}_-)^2\Delta^2\ln\frac{|\mu|+(\mu^2-\Delta^2)^{1/2}}{|\Delta|}\right\}, \tag{B6}$$

which depends on the electron chemical potential μ.

The TO phonon Green function $D''_{\rm TO}$ is defined by the diagrams in Figs. 6(e) and 6(f) where the mean-field approximation[13,45] is adopted and contributions either from

the first order in the quartic anharmonicity or from the second order in the cubic anharmonicities are retained.[64] This yields

$$D''_{\mathrm{TO}}(\mathbf{q};i\zeta_l)=\frac{1}{D'_{\mathrm{TO}}(\mathbf{q};i\zeta_l)^{-1}-\Pi_{\mathrm{TO}}(\mathbf{q};i\zeta_l)}=\frac{2\omega'_q}{\zeta_l^2+(\omega''_{\mathbf{q}})^2}\ , \tag{B7}$$

where

$$D'_{\mathrm{TO}}(\mathbf{q};i\zeta_l)=\frac{2\omega'_{\mathbf{q}}}{\zeta_l^2+(\omega'_{\mathbf{q}})^2}\ , \tag{B8}$$

$$\Pi_{\mathrm{TO}}(\mathbf{q};i\zeta_l)=-\sum_{j,\mathbf{k}}T\sum_n \mathrm{Tr}[(2\omega_0)^{1/2}\hat{g}^j(-\mathbf{q})\hat{G}^j_0(\mathbf{k};i\omega_n)\times(2\omega_0)^{1/2}\hat{g}^j(\mathbf{q})\times\hat{G}^j_0(\mathbf{k}-\mathbf{q};i\omega_n-i\zeta_l)]\ . \tag{B9}$$

Again, we have neglected small terms of the order ω_0/Δ, coming from the frequency dependence of Π_{TO}. The modified frequency of TO mode is obtained from (B7) in the form

$$(\omega''_{\mathbf{q}})^2=(\omega'_{\mathbf{q}})^2-2\omega'_{\mathbf{q}}\Pi_{\mathrm{TO}}(\mathbf{q};i0^+)\ . \tag{B10}$$

which may be rewritten as

$$(\omega''_0)^2=\omega_P^2+\tfrac{1}{2}\tilde{u}^2A+\tilde{\epsilon}B+\tfrac{1}{2}\tilde{\epsilon}^2C\ , \tag{B11}$$

at the Γ point in the rhombohedral phase. Taking the limit of vanishing order parameters, we can reproduce the expression of ω_P as given in Eq. (4.14) in the text.

Now we are going to consider the effects of the bilinear mode coupling proportional to the order parameter $\langle u\rangle$ according to the manner diagramatically shown in Figs. 6(a) and 6(b). Demanding the vanishing of the denominator of D_{TA} and D_{TO}, we have the frequencies of the coupled phonon modes as

$$\omega^2_{\mathbf{q}\pm}=\tfrac{1}{2}((\omega''_{\mathbf{q}})^2+q^2(s''_{\mathbf{q}})^2\pm\{[(\omega''_{\mathbf{q}})^2-q^2(s''_{\mathbf{q}})^2]^2+4q^2[\Pi_I(\mathbf{q};i0^+)]^2\}^{1/2})\ , \tag{B12}$$

which reduce in the limit $q\to 0$ to the expressions

$$\omega^2_{\mathbf{q}+}\to(\omega''_{\mathbf{q}})^2+q^2\delta\ \ as\ \mathbf{q}\to 0\simeq(\omega''_0)^2\equiv\omega_F^2\ , \tag{B13}$$

$$\frac{1}{q^2}\omega^2_{\mathbf{q}-}\to(s''_0)^2-\delta\ \ as\ \mathbf{q}\to 0\equiv s_F^2=\frac{1}{\rho}C_{44}^F\ , \tag{B14}$$

$$\delta=\frac{1}{\omega_F^2}[\Pi_I(0;i0^+)]^2\ , \tag{B15}$$

$$\Pi_I(0;i0^+)=-\tilde{u}B\ . \tag{B16}$$

In the same limit, the phonon Green functions including the effects of mode-mode coupling can be expressed as

$$D_{\mathrm{TA}}(\mathbf{q};i\zeta_l)\to\frac{2qs''_{\mathbf{q}}}{\zeta_l^2+\omega^2_{\mathbf{q}-}}\left[1-\frac{q^2\delta}{\omega^2_{\mathbf{q}+}-\omega^2_{\mathbf{q}-}}\right]+\frac{2qs''_{\mathbf{q}}}{\zeta_l^2+\omega^2_{\mathbf{q}+}}\frac{q^2\delta}{\omega^2_{\mathbf{q}+}-\omega^2_{\mathbf{q}-}}\ \text{as}\ \mathbf{q}\to 0\ , \tag{B17a}$$

$$D_{\mathrm{TO}}(\mathbf{q};i\zeta_l)\to\frac{2\omega''_{\mathbf{q}}}{\zeta_l^2+\omega^2_{\mathbf{q}+}}\left[1-\frac{q^2\delta}{\omega^2_{\mathbf{q}+}-\omega^2_{\mathbf{q}-}}\right]+\frac{2\omega''_{\mathbf{q}}}{\zeta_l^2+\omega^2_{\mathbf{q}-}}\frac{q^2\delta}{\omega^2_{\mathbf{q}+}-\omega^2_{\mathbf{q}-}}\ \text{as}\ \mathbf{q}\to 0\ . \tag{B17b}$$

The Green functions D_{TA} and D_{TO} look like the ones for the free phonons, except for that the frequencies are replaced by the renormalized expression in (B13) and (B14). It should be noted that the dispersion relation of the TO mode changes discontinuously at the transition, corresponding to the acoustic anomaly in the TA mode with abrupt appearance of the quantity δ.

APPENDIX C: VIBRONIC ANHARMONICITY AND SPIN-ORBIT COUPLING

This Appendix is devoted to an estimate of the magnitude of vibronic anharmonic effect to be compared with the lattice anharmonicity, taking explicit account of the spin-orbit coupling.

Let us consider the fourth-order vibronic contribution to the self-energy of TO phonons

$$\Pi_A=-\sum_j T\sum_n e^{i\omega_n 0^+}\sum_{\mathbf{k}}\mathrm{Tr}\{[(2\omega_0)^{1/2}\hat{g}^j(0)\hat{G}^j_0(\mathbf{k};i\omega_n)]^4\} \tag{C1a}$$

$$=-4\omega_0^2\sum_j(\mathbf{g}^j\cdot\mathbf{g}^j)\sum_{\mathbf{k}}\Theta[(\kappa^j)^2+\Delta^2-\mu^2]\left[\frac{1}{[\Delta^2+(\kappa^j)^2]^{3/2}}-6\frac{(\kappa_\perp^j)^2}{[\Delta^2+(\kappa^j)^2]^{5/2}}+5\frac{(\kappa_\perp^j)^4}{[\Delta^2+(\kappa^j)^2]^{7/2}}\right]\ , \tag{C1b}$$

where $\mathbf{g}^j$ is defined in Eq. (2.18) in the text, and $\kappa_\perp^j=|\boldsymbol{\kappa}^j\times\mathbf{g}^j|$. For simplicity, let us confine ourselves in the case of the fully occupied valence (completely empty conduction) band and put $\mu=\Delta$. Retaining only the lowest-order contribution in the parameter Δ/κ_0, the Eq. (C1b) is calculated to yield

$$\frac{1}{6\pi^2(NM)^2v_\parallel v_\perp^2}\left[\Xi_\parallel^4+3\left[\frac{\Xi_\parallel^2+8\Xi_\perp^2}{9}\right]^2\right]\left[\ln\frac{2\kappa_0}{|\Delta|}+\frac{229}{15}\right]>0\ . \tag{C2}$$

The corresponding result for Kane's isotropic two-band model[65] is reproduced by putting $\kappa_{\perp}^{j}=0$ and $\kappa_{\parallel}^{j}=\kappa^{j}$;[66]

$$-\frac{14}{81\pi^2(NM)^2v^3}\Xi_{\rm op}^4\ln\frac{2\kappa_0}{|\Delta|}<0\ , \tag{C3}$$

where $v_{\parallel}$ and $v_{\perp}$ in Eq. (C2) are replaced by the isotropic velocity v, and $\Xi_{\parallel}$ by $\Xi_{\rm op}$ while $\Xi_{\perp}$ is 0. It should be noted that the spin-orbit coupling changes the sign of the vibronic contribution in the isotropic bands. When we include this vibronic contribution in our theory, the lattice anharmonic constant A is renormalized to $A-6\Pi_A$. Furthermore, if the vibronic contribution is assumed to be dominant compared with A, the coefficient β in Eq. (4.17c) becomes always negative, predicting the first-order instead of the observed second-order transition.[50] Finally, we note that such a competition between vibronic and lattice anharmonicity is absent in the isotropic two-band model, since both give definitely positive contributions.[2,67] Thus the anisotropy of electron bands becomes important when the electron—TO-phonon coupling is present because it has the interband matrix elements. Moreover the spin-orbit coupling causes a correlation between velocity matrix elements and a coupling constant of electron—TO-phonon interaction.

[1]J. F. Scott, Rev. Mod. Phys. **46**, 83 (1974).

[2]I. B. Bersuker and B. G. Vekhter, Ferroelectrics **19**, 137 (1978).

[3]H. Kawamura, in *Narrow-Gap Semiconductors, Physics and Applications,* Vol. 133 of *Lecture Notes in Physics,* edited by W. Zawadzki (Springer, Berlin, 1980), p. 470.

[4]G. Nimtz and B. Schlicht, in *Narrow-Gap Semiconductors,* Vol. 98 of *Springer Tracts in Modern Physics,* edited by G. Höhler (Springer, Berlin, 1983), p. 1.

[5]W. Jantsch, in *Dynamical Properties of IV-VI Compounds,* Vol. 99 of *Springer Tracts in Modern Physics,* edited by G. Höhler (Springer, Berlin, 1983), p. 1.

[6]A. Bussmann-Holder, H. Biltz, and P. Vogl, in *Dynamical Properties of IV-VI Compounds,* Vol. 99 of *Springer Tracts in Modern Physics,* Ref. 5, p. 51.

[7]S. Katayama and D. L. Mills, Phys. Rev. B **19**, 6372 (1979).

[8]S. Katayama and D. L. Mills, Phys. Rev. B **22**, 336 (1980).

[9]S. Takaoka and K. Murase, J. Phys. Soc. Jpn. **51**, 1857 (1982).

[10]S. Takaoka and K. Murase, Phys. Rev. B **20**, 2823 (1979).

[11]A. Bussmann-Holder, H. Biltz, and P. Vogl, in *Dynamical Properties of IV-VI Compounds,* Vol. 99 of *Springer Tracts in Modern Physics,* Ref. 5, Sec. 3.5, and references therein.

[12]J. C. Slonczewski and H. Thomas, Phys. Rev. B **1**, 3599 (1970).

[13]E. Pytte, Phys. Rev. B **5**, 3758 (1972).

[14]R. B. Griffiths, Phys. Rev. Lett. **24**, 715 (1970).

[15]R. Clarke, Phys. Rev. B **18**, 4920 (1978).

[16]N. Kristoffel and P. Konsin, Ferroelectrics **6**, 150 (1973), and references therein.

[17]I. B. Bersuker and B. G. Vekhter, Ferroelectrics **19**, 137 (1978), and references therein.

[18]H. Kawamura, S. Katayama, S. Takaoka, and S. Hotta, Solid State Commun. **14**, 259 (1974).

[19]W. Porod and P. Vogl, in *Proceedings of the 4th International Conference on Physics of Narrow Gap Semiconductors, Linz, 1981,* Vol. 152 of *Lecture Notes in Physics,* edited by E. Gornik, H. Heinrich, and L. Palmetshofer (Springer, New York, 1982), p. 247.

[20]A. Bussmann-Holder, H. Biltz, and P. Vogl, in *Dynamical Properties of IV-VI Compounds,* Vol. 99 of *Springer Tracts in Modern Physics,* Ref. 5, Sec. 3.2.

[21]W. Jantsch, in *Dynamical Properties of IV-VI Compounds,* Vol. 99 of *Springer Tracts in Modern Physics,* Ref. 5, Sec. 5.2.

[22]A. Bussmann-Holder, H. Biltz, and P. Vogl, in *Dynamical Properties of IV-VI Compounds,* Vol. 99 of *Springer Tracts in Modern Physics,* Ref. 5. Sec. 3.

[23]G. Nimtz and B. Schlict, in *Narrow-Gap Semiconductors,* Vol. 98 of *Springer Tracts in Modern Physics,* Ref. 4, Sec. 3.1.

[24]D. L. Mitchell and R. F. Wallis, Phys. Rev. **151**, 581 (1966).

[25]P. A. Wolff, J. Phys. Chem. Solids **25**, 1057 (1964).

[26]K. Murase, Proceedings of the 15th International Conference on Physics of Semiconductors, Kyoto, 1980 [J. Phys. Soc. Jpn. **49**, Suppl. A, 725 (1980)].

[27]K. L. I. Kobayashi, Y. Kato, Y. Katayama, and K. F. Komatsubara, Phys. Rev. Lett. **37**, 772 (1976).

[28]K. Murase and S. Nishi; *Proceedings of the 4th International Conference on Physics of Narrow Gap Semiconductors, Linz, 1981,* Vol. 152 of *Lecture Notes in Physics,* Ref. 19, p. 261.

[29]T. Seddon and S. C. Gupta, Solid State Commun. **20**, 69 (1976).

[30]A. Natori, J. Phys. Soc. Jpn. **40**, 163 (1976).

[31]V. I. Litvinov, V. L. Volkov, and V. K. Dugaev, Fiz. Tverd. Tela (Leningrad) **22**, 57 (1980) [Sov. Phys.—Solid State **22**, 32 (1980)].

[32]K. Sakai, Proceedings of the 6th International Meeting on Ferroelectricity, Kobe, 1985 [Jpn. J. Appl. Phys. **24**, 189 (1985)].

[33]S. Rabii, Phys. Rev. **182**, 821 (1969).

[34]Y. W. Tung and M. L. Cohen, Phys. Lett. **A29**, 236 (1969).

[35]Y. W. Tung and M. L. Cohen Phys. Rev. **180**, 823 (1969).

[36]J. S. Melvin and D. C. Hendry, J. Phys. C **12**, 3003 (1979).

[37]H. M. Polatoglou, G. Theodorou, and N. A. Economou; *Proceedings of the 4th International Conference on Physics of Narrow Gap Semiconductors, Linz, 1981,* Vol. 152 of *Lecture Notes in Physics,* Ref. 19, p. 221.

[38]V. K. Dugaev, V. L. Volkov, V. I. Litvinov, and K. D. Tovstyuk, Fiz. Tverd. Tela (Leningrad) **20**, 2015 (1978) [Sov. Phys.—Solid State **20**, 1163 (1978)].

[39]J. W. McClure and J. Martyniuk, Phys. Rev. Lett. **29**, 1095 (1972).

[40]J. W. McClure, I. V. Svechkarev, and G. E. Grechnev, Fiz. Nizk. Temp. **4**, 1534 (1978) [Sov. J. Low Temp. Phys. **4**, 722 (1978)].

[41]J. M. Luttinger and W. Kohn, Phys. Rev. **97**, 869 (1955).

[42]J. D. Bjorken and S. D. Drell, *Relativistic Quantum Mechanics* (McGraw-Hill, New York, 1964), Appendix A.

[43]In the preliminary report (Ref. 32), we have incorporated the third-order anharmonic coupling of the TA mode which gives a third-order elastic constant C_{456} [R. F. S. Hearmon; Acta Cryst. **6**, 331 (1953)]. But this effect is negligibly small and is neglected here.

[44]J. M. Ziman, *Electrons and Phonons* (Clarendon, London, 1967), Sec. 5. 10.

[45]E. Pytte, Phys. Rev. Lett. **28**, 895 (1972).

[46]W. Jantsch, in *Dynamical Properties of IV-VI Compounds,* Vol. 99 of *Springer Tracts in Modern Physics,* Ref. 5, Sec. 5. 1., Table 5. 1.

[47]A. Bussmann-Holder, H. Biltz, and P. Vogl, in *Dynamical Properties of IV-VI Compounds,* Vol. 99 of *Springer Tracts in Modern Physics,* Ref. 5, Sec. 3. 5.1, p. 83.

[48]An erroneous condition in our preliminary report (Ref. 32) should be revised here: The reduced temperature τ_a should be interpreted as τ_b in the present paper.

[49]S. Sugai, K. Murase, T. Tsuchihira, and H. Kawamura, J. Phys. Soc. Jpn. **47**, 539 (1979).

[50]M. Iizumi, Y. Hamaguchi, K. F. Komatsubara, and Y. Kato, J. Phys. Soc. Jpn. **38**, 443 (1975).

[51]K. Inoue and N. Asai, J. Phys. (Paris) Colloq. **42**, C6-430 (1981).

[52]S. Rabii, Phys. Rev. **182**, 821 (1969).

[53]L. G. Ferreira, Phys. Rev. **137**, A1601 (1965).

[54]L. Muldawer, J. Nonmetals **1**, 177 (1973).

[55]J. de Launay, in *Solid State Physics,* edited by F. Seitz and D. Turnbull (Academic, New York, 1956), Vol. 2, Chap. XI, p. 219.

[56]H. Kawamura, S. Nishikawa, and K. Murase; in *Proceedings of the International Conference on Applications of High Magnetic Fields in Semiconductor Physics,* edited by J. F. Ryan (Oxford University, New York, 1978), p. 170.

[57]R. W. Keyes, in *Solid State Physics,* edited by F. Seitz, D. Turnbull, and H. Ehrenreich, Ref. 55, Vol. 20, p. 37.

[58]A. K. Sreedhar and S. C. Gupta, Phys. Rev. B **5**, 3160 (1972).

[59]S. Nishikawa, Ph. D. thesis, Osaka University, 1979.

[60]S. Takaoka, Ph. D. thesis, Osaka University, 1979.

[61]G. Nimtz and B. Schlicht, in *Narrow-Gap Semiconductors,* Vol. 98 of *Springer Tracts in Modern Physics,* Ref. 4, Sec. 3.2.3.1, Fig. 3. 11.

[62]J. Bardeen and W. Shockley, Phys. Rev. **80**, 72 (1950).

[63]F. S. Khan and P. B. Allen, Phys. Rev. B **29**, 3341 (1984).

[64]A. A. Maradudin and A. E. Fein, Phys. Rev. **128**, 2589 (1962).

[65]E. O. Kane, in *Semiconductors and Semimetals,* Vol. 1 of *Physics of III-V Compounds,* edited by R. K. Willardson and A. C. Beer (Academic, New York, 1966), Chap. 3.

[66]In case that the spin-orbit coupling does not play an important role, we may smear out the anisotropy in the spectrum induced by the spin-orbit coupling and obtain an isotropic spectrum same as Kane's isotropic two-band model (Ref. 65). This is done by an angle average of Hamiltonian (2.5), i.e., by a replacement of the elements of the modified crystal momentum $(\kappa_1^j,\kappa_2^j,\kappa_3^j)$ by $(0,0,\kappa^j)$, where $(\kappa^j)^2=(\kappa_1^j)^2+(\kappa_2^j)^2+(\kappa_3^j)^2$.

[67]Ya. G. Girshberg and V. I. Tamarchenko, Fiz. Tverd. Tela (Leningrad) **18**, 1066 (1976) [Sov. Phys.—Solid State **18**, 609 (1976)].

[68]S. Sugai, K. Murase, S. Katayama, S. Takaoka, S. Nishi, and H. Kawamura, Solid State Commun. **24**, 407 (1977).